Computational Materials Science xxx (xxxx) 114397

Contents lists available at ScienceDirect

Computational Materials Science

journal homepage: www.elsevier.com/locate/commatsci

Lattice constant prediction of ABX_3 and $A_2BB'X_6$ perovskites using autoregressive type 3 fuzzy model optimized by extended Kalman filter

Mohammed Assam Ouali [a], Hamza Bennacer [a, b, *], Mohamed Ladjal [a, c], Inas Bouzateur [d]

[a] Department of Electronics, Faculty of Technology, University of M'Sila, 28000 M'Sila, Algeria
[b] Elaboration and Physico-Mechanical and Metallurgical Characterization of Materials Laboratory, ECP3M, University of Mostaganem, Algeria
[c] LASS, Laboratory of Analysis of Signals and Systems, University of M'sila, Algeria.
[d] Laboratory for Modeling and Simulation of Magnetic Properties Hetero-structures, Science and Technology Faculty, Tissemsilt University, 38000 Tissemsilt, Algeria.

ARTICLE INFO

Keywords:
Perovskites and double perovskites
Lattice constant prediction
Machine learning in materials science
Autoregressive modeling
Type-3 fuzzy logic
Extended Kalman filter

ABSTRACT

Predicting lattice constants is critical to advancing the discovery of functional materials. When dealing with highly nonlinear data, traditional techniques, such as Density Functional Theory (DTF), frequently suffer from restricted generalization and high computational cost. This study presents a hybrid predictive framework that merges an Autoregressive Type-3 Fuzzy Logic System with the Extended Kalman Filter (AR-T3FLS-EKF) to overcome these constraints and address the issue of restricted and scarce data. The autoregressive technique incorporates physical dependencies among compositional descriptors, whereas the Type-3 fuzzy system improves uncertainty modeling using three-dimensional membership functions. The extended kalman filter adaptively tunes the fuzzy model parameters, improving robustness and convergence. The proposed model is validated on three datasets of perovskite and double perovskite structures using features such as ionic radii, electronegativity, and tolerance factor. Compared with conventional machine learning methods, the AR-T3FLS-EKF achieves superior performance ($R^2 = 0.9999$, $MAE = 0.0015$ Å, $RMSE = 0.0012$ Å). These results confirm the model's reliability for accurate lattice constant prediction, especially under limited and scarce data conditions.

1. Introduction

Materials have consistently been essential in the advancement of human civilization, propelling advances in technology, industry, and quality of life. The discovery and optimization of materials has allowed for advancements in vital fields like energy, healthcare, transportation, and communication, starting with the earliest tools in ancient cultures and continuing through today's state-of-the-art semiconductors and nanomaterials. The need for cutting-edge materials with better structural, mechanical, electrical, optical, and thermal qualities is growing as civilization moves toward more complex technology. Furthermore, tackling global issues like efficient manufacturing, environmental preservation, and sustainable energy relies heavily on the capacity to develop customized materials [1–4]. Materials are thus still essential to innovation, industrial change, and the creation of high-performing solutions for a world that is changing quickly.

The axe of research and development is material science, which connects between numerous fields such as physics, chemistry, and practical engineering applications. Researchers can develop new compounds with the appropriate functionalities by studying the relationship between the atomic structure of material and its physical features [4]. However, experimental procedures are frequently time-consuming and costly, necessitating substantial synthesis and characterization processes. Computational techniques based on artificial intelligence, has emerged as powerful tools to discover novel materials by predicting attributes before building new component [5,6].

Among the most attractive materials in current technology are perovskites and double perovskites, which are a family of compounds with ABO_3 and $A_2BB'X_6$ formula respectively [5–9]. Perovskite and double perovskite materials are promising compounds for next-generation technologies like solar photovoltaics, thermoelectric converters, light-emitting diodes, and sensors because of their special physical properties, including electronic, optical, and thermal features [10]. Specifically, perovskite solar cells have transformed photovoltaics by outperforming conventional silicon-based technologies and attaining remarkable power conversion efficiencies. Their compositional flexibility allows for adjustments that improve performance or minimize environmental impact, aligning well with the rising need for green and cost-effective materials [10–12].

* Corresponding author at: Department of Electronics, Faculty of Technology, University of M'Sila, 28000 M'Sila, Algeria.
E-mail address: hamza.bennacer@univ-msila.dz (H. Bennacer).

https://doi.org/10.1016/j.commatsci.2025.114397
Received 2 September 2025; Received in revised form 31 October 2025; Accepted 17 November 2025
0927-0256/

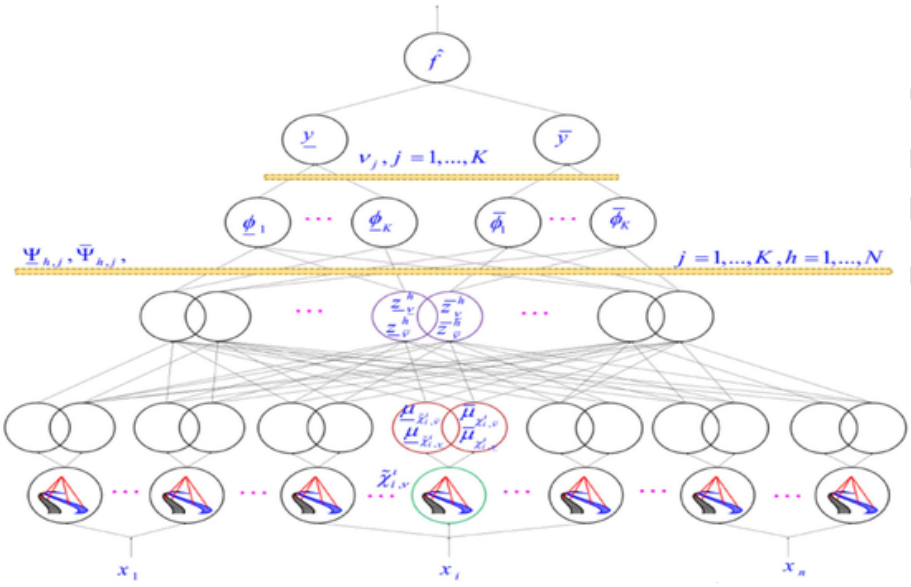

Fig. 1. Type 3 fuzzy logic system [80].

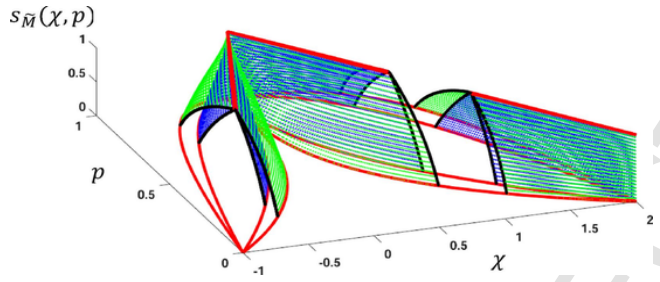

Fig. 2. Type 3 fuzzy membership function.

The Lattice constant parameter defines the crystallographic dimensions of a material's unit cell and reflects the geometric configuration of atoms within the crystal structure, and is an important consideration in the design and selection of materials for photovoltaic (PV) cells, optoelectronic, and electronic applications. In thin films and heterostructures, the lattice constant parameter has a direct impact on interfacial matching, thermal expansion, phase stability, and mechanical strength. Moreover, this parameter is crucial for reducing interfacial recombination and enhancing device performance in semiconductor heterostructures utilized in optoelectronic devices. Therefore, developing next-generation thin-film technologies through the accurate prediction of the lattice constant parameter is essential to creating electrical and optoelectronic devices that are more effective and durable [13,14].

In complex compounds such as perovskites ABO_3 and double perovskites $A_2BB'X_6$, the slight variations in lattice constant parameters alter significantly their functional properties, including optical absorption, ionic conductivity, and magnetic behavior. Moreover, accurate knowledge of lattice parameters is essential for guiding synthesis conditions and ensuring lattice matching in hetero-structure elaboration, where interfacial strain can affect device performance. Lattice constants are fundamental characteristics used in computational materials research to describe and screen potential materials across wide compositional space. Thus, building predictive models that can estimate lattice constants with high precision is not only beneficial for expediting materials discovery, but also for enhancing material performance in energy, electronics, and structural applications [15–17].

Perovskite and double Perovskite materials are known for their complex physical and chemical structures, this complexity presents considerable difficulties for precise modeling and predicting of their characteristics. Due to the intrinsic versatility of the perovskite structure, a vast range of elemental substitutions may occur at both the A and B sites, resulting in a rich variety of physical characteristics such as ferroelectricity, superconductivity, and photovoltaic activity. By adding two different cations to the B-site, double perovskites add another level of complexity to their behavior. This frequently leads to structural distortions, charge ordering, and spin interactions. Features such as the electronic arrangement of constituent ions, the tolerance factor, and the ionic radii all affect these compounds' symmetry, stability, and lattice constants. Perovskite materials are extremely adjustable due to their structural flexibility, but this also presents non-linear correlations between composition and attributes that are challenging to describe with traditional empirical or purely computational approaches. Therefore, to reliably predict the lattice parameters and other structural features of these complex compounds, efficient predictive models that can deal with uncertainty, non-linearity, and interaction among descriptors are needed [18–26].

Despite the increasing demand for accurate and efficient prediction of lattice constants in perovskite and double perovskite materials, current computational and data-driven approaches face significant limitations. Density Functional Theory (DFT) [27,28], while widely used, is computationally expensive and often impractical for large-scale materials screening [29]. On the other hand, conventional machine learning models can offer faster predictions but generally struggle with generalization, interpretability, overfitting, and poor handling of data uncertainty especially in structurally diverse systems like perovskites and double perovskites [5–9] [15,30–44]. Moreover, existing fuzzy logic-based models, such as Type-1 and Type-2 fuzzy logic systems, lack the flexibility to represent the complex, high-level uncertainties present in experimental or computed materials data. Additionally, most predictive models overlook the physical or sequential dependencies in compositional descriptors that can be exploited for improved accuracy. These challenges highlight the need for a hybrid, interpretable, and adaptive modeling approach capable of capturing both the non-linear relationships and the uncertainty inherent in lattice constant prediction for structurally complex materials. In this context, researchers have increasingly turned to machine learning models [5–9] [15,30–44]. One

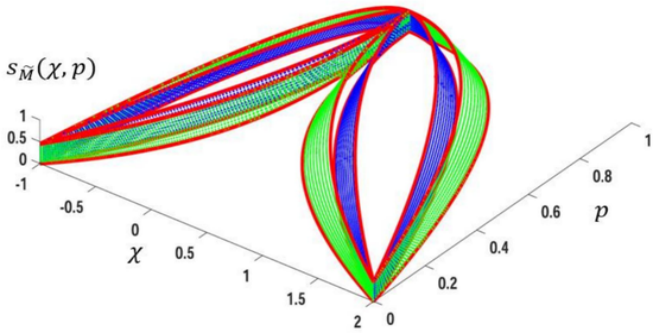

Fig. 3. The horizontal slice of the used membership function.

notable contribution involves the integration of artificial neural networks (ANN) and fuzzy logic systems, enhanced by metaheuristic optimization algorithms such as Particle Swarm Optimization (PSO), Invasive Weed Optimization (IWO), and Imperialist Competitive Algorithm (ICA), to predict lattice constants with improved accuracy has proposed by Bouzateur et al. [5]. Alfares et al. [6] applied machine learning models including SVR, GPR, ANN, and ERT; for lattice constant prediction in perovskites, using descriptors such as ionic radii and electronegativity. Optimized via Bayesian methods, the GPR model achieved exceptional accuracy (R^2 = 99 % on test data), outperforming other techniques. Their work demonstrates the effectiveness of ML, particularly GPR, as a scalable alternative to traditional computational methods in materials design. Other studies have extended machine learning applications in perovskites beyond structural parameters to electronic properties such as band gap prediction [30]. Researchers identified important variables like valence charge variation and obtained good accuracy in both regression and classification tasks using models like Random Forest and Adaptive Boosting Regression. The reported results underscore the extensive potential of machine learning in expediting the identification and improvement of perovskites for optoelectronic applications [30]. Alharthi et al. [31] proposed a very accurate artificial neural network model to predict lattice constant parameters in aliovalently doped perovskites and tackled the interpretability issue by utilizing Partial Dependence Plots (PDPs). This method revealed how structural elements affect predictions. Their findings emphasize the relevance of prediction performance and explain ability in machine learning-driven materials design. Ionic radius-based analytical and correlative models for perovskite lattice constant prediction are another area of investigation. A revised empirical equation with the lowest mean absolute relative error on high-quality structural datasets was proposed [32]. Using extensive datasets, XGBoost and Random Forest models classified and predicted structural and energetic features of halide and oxide perovskites in [33]. The models accurately predicted band gaps, formation energies, and stable perovskite solar cells. A feature significance analysis showed that d-electron count in the B-site atom is crucial for material optimization [33]. Yao et al. [34] proposed a data-driven methodology via hybrid artificial rabbits optimization and random forest regression to predict the dielectric constant of ABO_3 compounds. They identified critical dielectric behavior characteristics using enhanced feature selection and SHAP-based interpretability. The model demonstrated strong prediction ability (R^2 = 0.95), enabling the selection of prospective dielectric materials from a large candidate solution. Sabagh Moeini et al. [35] showed that machine learning methods including Support Vector Regression (SVR), Random Forest, Gradient Boosting, and XGBoost accurately estimate direct and indirect band gaps in low-symmetry double and multilayer perovskites. They found that SVR performed best overall and XGBoost excelled for double perovskites when derivative discontinuity was incorporated. Using six ML models, including CatBoost, XGBoost, and CompoundNet, Obada et al. [36] predicted band gaps in ABX_3 perovskites using elemental parameters including electronegativity and ionization energy. SHAP analysis showed that the B-site cation's electronegativity was most important. Finally, CatBoost and Boost have achieved high performance with $R^2 \geq 88$ %. Based on elemental characteristics, Jarin et al. [37] built

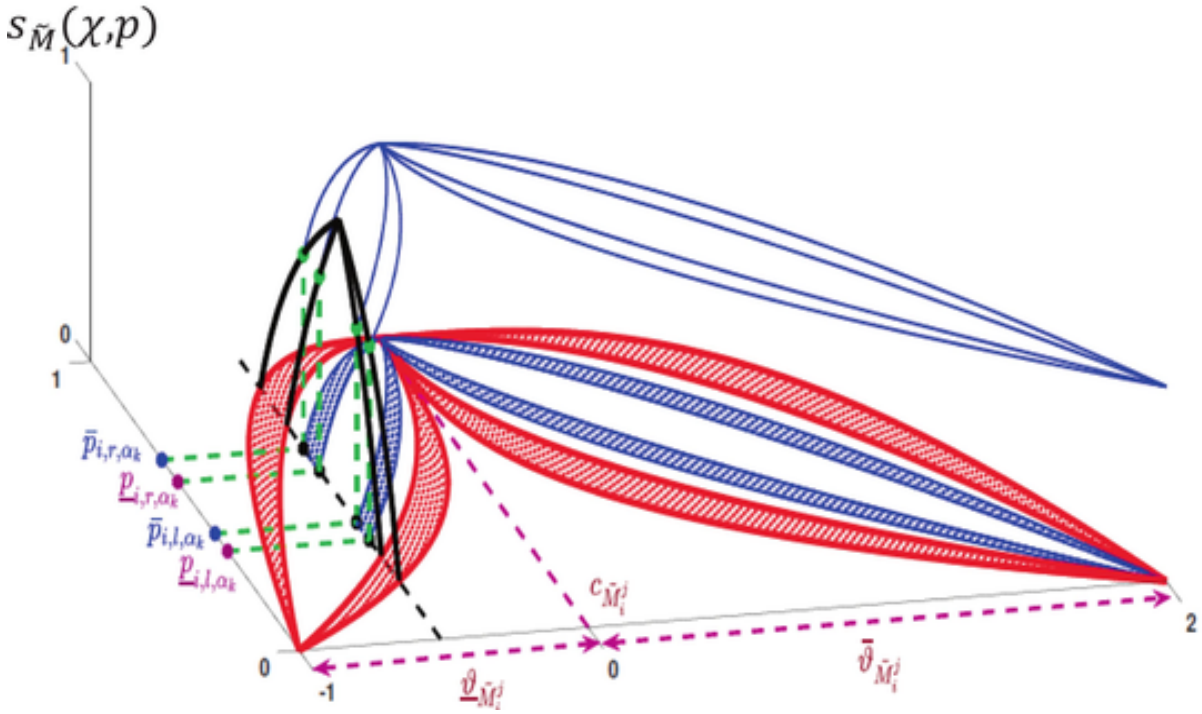

Fig. 4. The FOU for the type-3 membership function. [80].

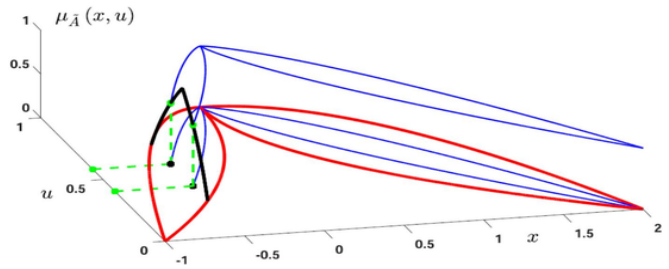

Fig. 5. The FOU for general type-2 membership function.

$$\overline{p}_{i,r,\alpha_k} = \begin{cases} 1-\left(\dfrac{x_i - c_{\widetilde{M}_i^j}}{\underline{\vartheta}_{\widetilde{M}_i^j}}\right)^{\Delta_r(1-\alpha_k)+1} & if\ c_{\widetilde{M}_i^j} - \underline{\vartheta}_{\widetilde{M}_i^j} < x_i \le c_{\widetilde{M}_i^j} \\ 1-\left(\dfrac{x_i - c_{\widetilde{M}_i^j}}{\overline{\vartheta}_{\widetilde{M}_i^j}}\right)^{\Delta_r(1-\alpha_k)+1} & if\ c_{\widetilde{M}_i^j} < x_i \le c_{\widetilde{M}_i^j} + \overline{\vartheta}_{\widetilde{M}_i^j} \\ 0 & if\ x_i > c_{\widetilde{M}_i^j} + \overline{\vartheta}_{\widetilde{M}_i^j}\ or\ x_i \le c_{\widetilde{M}_i^j} - \underline{\vartheta}_{\widetilde{M}_i^j} \end{cases} \tag{5}$$

$$\underline{p}_{i,r,\alpha_k} = \begin{cases} 1-\left(\dfrac{x_i - c_{\widetilde{M}_i^j}}{\underline{\vartheta}_{\widetilde{M}_i^j}}\right)^{1/\Delta_r(1-\alpha_k)+1} & if\ c_{\widetilde{M}_i^j} - \underline{\vartheta}_{\widetilde{M}_i^j} < x_i \le c_{\widetilde{M}_i^j} \\ 1-\left(\dfrac{x_i - c_{\widetilde{M}_i^j}}{\overline{\vartheta}_{\widetilde{M}_i^j}}\right)^{1/\Delta_r(1-\alpha_k)+1} & if\ c_{\widetilde{M}_i^j} < x_i \le c_{\widetilde{M}_i^j} + \overline{\vartheta}_{\widetilde{M}_i^j} \\ 0 & if\ x_i > c_{\widetilde{M}_i^j} + \overline{\vartheta}_{\widetilde{M}_i^j}\ or\ x_i \le c_{\widetilde{M}_i^j} - \underline{\vartheta}_{\widetilde{M}_i^j} \end{cases} \tag{6}$$

$$\overline{p}_{i,l,\alpha_k} = \begin{cases} 1-\left(\dfrac{x_i - c_{\widetilde{M}_i^j}}{\underline{\vartheta}_{\widetilde{M}_i^j}}\right)^{\Delta_l(1-\alpha_k)+1} & if\ c_{\widetilde{M}_i^j} - \underline{\vartheta}_{\widetilde{M}_i^j} < x_i \le c_{\widetilde{M}_i^j} \\ 1-\left(\dfrac{x_i - c_{\widetilde{M}_i^j}}{\overline{\vartheta}_{\widetilde{M}_i^j}}\right)^{\Delta_l(1-\alpha_k)+1} & if\ c_{\widetilde{M}_i^j} < x_i \le c_{\widetilde{M}_i^j} + \overline{\vartheta}_{\widetilde{M}_i^j} \\ 0 & if\ x_i > c_{\widetilde{M}_i^j} + \overline{\vartheta}_{\widetilde{M}_i^j}\ or\ x_i \le c_{\widetilde{M}_i^j} - \underline{\vartheta}_{\widetilde{M}_i^j} \end{cases} \tag{7}$$

$$\underline{p}_{i,l,\alpha_k} = \begin{cases} 1-\left(\dfrac{x_i - c_{\widetilde{M}_i^j}}{\underline{\vartheta}_{\widetilde{M}_i^j}}\right)^{1/\Delta_l(1-\alpha_k)+1} & if\ c_{\widetilde{M}_i^j} - \underline{\vartheta}_{\widetilde{M}_i^j} < x_i \le c_{\widetilde{M}_i^j} \\ 1-\left(\dfrac{x_i - c_{\widetilde{M}_i^j}}{\overline{\vartheta}_{\widetilde{M}_i^j}}\right)^{1/\Delta_l(1-\alpha_k)+1} & if\ c_{\widetilde{M}_i^j} < x_i \le c_{\widetilde{M}_i^j} + \overline{\vartheta}_{\widetilde{M}_i^j} \\ 0 & if\ x_i > c_{\widetilde{M}_i^j} + \overline{\vartheta}_{\widetilde{M}_i^j}\ or\ x_i \le c_{\widetilde{M}_i^j} - \underline{\vartheta}_{\widetilde{M}_i^j} \end{cases} \tag{8}$$

machine learning algorithms to predict perovskite crystal structures and lattice constant parameters. The hybrid GA-NN model achieved an accuracy of 88 % for crystal structure classification, while the GA-SVR model achieved an accuracy of 95 % for lattice constant parameter prediction. Data-driven structural distortion prediction by these methods may speed perovskite discovery and design. Perovskite material discovery using machine learning has been extensively reviewed. This review examined publication trends, ML procedures, and inorganic, hybrid, and double perovskites applications. In addition, it suggested interesting future avenues to improve ML-driven materials innovation, presenting ML as a transformational tool in perovskite research [38]. Partial least squares and principal component regression methods were used to estimate the lattice constants of ABX_3 and $A_2BB'O_6$ perovskites utilizing features including Shannon ionic radii, atomic number, electronegativity, and density [39]. In their Random Forest-based machine learning model, Li et al. [40] predicted lattice constant parameters and angles of crystalline materials using just their molecular formulas. By integrating a novel descriptor set, the model achieved an impressive R^2 of 0.973 for the lattice constant parameter in cubic crystals and an average R^2 of 0.80 across all crystal systems. Unlike earlier models limited by small datasets or material-specific focus, MLatticeABC demonstrated broader applicability and improved accuracy, especially for diverse crystal systems. The approach also showed notable gains in predicting lattice angles, with the code and models made openly available. Zhang et al. [41] used ionic radii and electronegativities to predict cubic metal halide perovskites' lattice constants using Gaussian Process Regression (GPR). Using 79 samples with lattice constants from 8.109 to 11.790 Å, the model showed remarkable accuracy and stability. This method is fast, robust, and cost-effective for calculating structural factors that affect perovskite-based device performance and efficiency. Ionic radii and electronegativity were used to construct a Support Vector Regression model for cubic A_2XY_6 crystals to enhance lattice constant prediction. SVR minimized prediction errors compared to linear models. This shows SVR's ability to capture nonlinear crystal structure interactions and speed up materials discovery [15]. Williams et al. [42] use modified Hirschfeld surface fingerprints and deep learning to predict cubic inorganic perovskites' lattice constant parameters. Capturing intricate geometric and bonding elements. This method is promise for data-driven, high-throughput crystal structure prediction. Many other contributions have been proposed in the literature and reported in various research studies [8,11] [43–51].

Type-3 fuzzy logic extends traditional fuzzy logic by introducing a third level of uncertainty, capturing both membership ambiguity and the uncertainty in the degree of fuzziness itself [52,53]. This makes it especially useful in modeling highly imprecise, noisy, or vague systems.

Table 1
Comparative study between Mamdani and the used fuzzy inference system.

Parameters	Mamdani FIS	Used FIS	Observation
Rule output type	Fuzzy sets	Mathematical functions (crisp values)	The used FIS avoids defuzzification step
Defuzzification requirement	Required (Mamdani FIS is slower because of the complex nature of the defuzzification process)	Not required (The used FIS is Faster)	Simlpifies Computation
Computational complexity	Relatively high	Lower	Suitable for online or real time systems
Adaptability for optimization	Limited	Excellent	Rule parameters easily tuned using optimization or learning algorithms
Suitability for integration with EKF	Limited	High	The used FIS integrates seamlessly with mathematical models
Typical applications	Control systems requiring human like reasoning	Adaptive modeling, prediction, and hybrid systems.	The used FIS better for data driven modeling
Scalability	Limited scalability; complexity grows rapidly with number of inputs and rules	Highly scalable; computational load increases linearly with inputs	Proposed system maintains efficiency for large-scale or high-dimensional problems

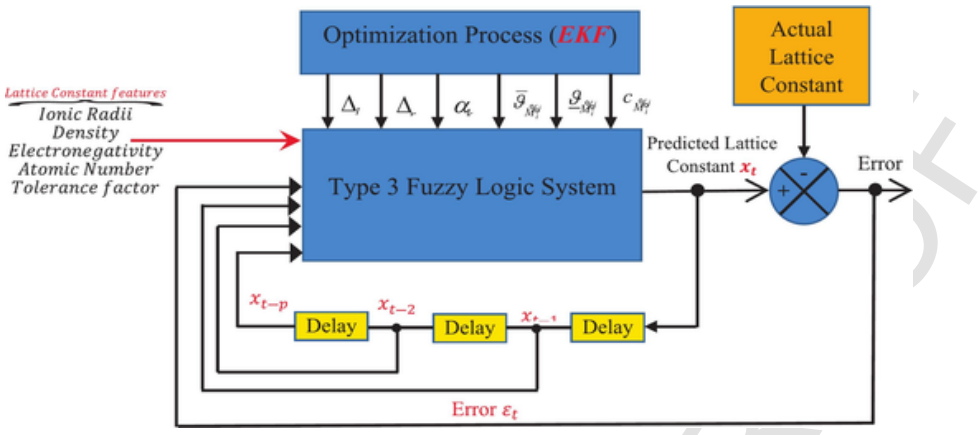

Fig. 6. Proposed autoregressive type-3 fuzzy logic model for lattice constant prediction of perovskite materials.

Table 2
Initial parameters of the type-3 fuzzy membership functions before EKF tuning.

Parameters	Initial values
Centers of MFs	$c_{\tilde{M}_i^1} = -1$, $c_{\tilde{M}_i^2} = 0$ and $c_{\tilde{M}_i^3} = 1$
Width of upper MFs	$\Delta_r = 3$
Width of lower MFs	$\Delta_l = 2$
Right distance	$\overline{\vartheta}_{\tilde{M}_i^1} = 2$, $\overline{\vartheta}_{\tilde{M}_i^2} = 1$ and $\overline{\vartheta}_{\tilde{M}_i^3} = 2$
Left distance	$\underline{\vartheta}_{\tilde{M}_i^1} = 1$, $\underline{\vartheta}_{\tilde{M}_i^2} = 2$ and $\underline{\vartheta}_{\tilde{M}_i^3} = 1$
Alpha-cuts	two horizontal slice is considered $\alpha = 0.5$ and $\alpha = 0.8$

In predictive tasks, Type-3 fuzzy logic enhances robustness by handling complex nonlinearities and uncertain input data more effectively than Type-1 or Type-2 systems. It has found applications in time-series prediction, system identification, and sensor fusion. By incorporating autoregressive structures, Type-3 fuzzy systems can learn physical dependencies for dynamic predictions [54,55]. These capabilities make it a powerful tool for improving accuracy and interpretability in challenging prediction problems. The effectiveness of Type-3 fuzzy logic has drawn significant interest from researchers, leading to the development of various techniques for time series prediction using this advanced tool [7,9,56–63].

Compared to type-2 and type-1 fuzzy logic systems, type 3 fuzzy logic performs better when modeling extremely complicated cases. For instance, a type 3 logic system can better adapt to various cases and offer more accurate modeling for problems with multiple variables and inputs, as well as high complexity. Furthermore, for multi-objective decision issues, the type 3 fuzzy logic system method can account the impacts of ambiguous information and lead to better prioritisation. Many studies have demonstrated the superiority of T3-FLSs. The fundamental reason is that T3-FLSs have a higher degree of freedom to represent uncertainty. In addition to the fact that the secondary fuzzy set is not a distinctive number in T3-FLSs, the footprint-of-uncertainty is a fuzzy set. Because of the interval structure of the primary and secondary membership functions, the type-3 fuzzy system is more suited to modeling uncertain information and data. It also includes a third domain, namely, unity tertiary membership. Type-3 fuzzy systems provide a greater number of control parameters that can be tuned during model building than other fuzzy systems (types 1 and 2). Thus, type 3 fuzzy systems have a higher degree of freedom to account for data uncertainty.

The Extended Kalman Filter (EKF) is a recursive technique used to estimate the state of nonlinear systems by linearizing around the actual estimate [64]. It extends the standard Kalman filter by using a first-order Taylor series expansion to handle nonlinear models, and is a reliable approach for iteratively tuning parameter estimations in optimization problems by minimizing the difference between anticipated and actual values [65–67]. EKF is frequently utilized in control systems, robotics, and machine learning because of its flexibility to real-time and noisy situations [68–72]. Because of its predictive-corrective structure, it can adapt to new data as it becomes available. EKF is an effective technique for optimizing models with uncertain and nonlinear variable relationships.

The effectiveness of type-3 fuzzy logic systems combined with Kalman filter techniques has been well demonstrated in the literature. This hybridization leverages the strong uncertainty modeling capability of type-3 fuzzy systems and the dynamic estimation strength of Kalman filter. *Sultan* et al. [73] developed a self-organizing interval Type-3 fuzzy logic system (SO-IT3FLS) with an adaptive learning algorithm that enhances the robustness of correntropy-based Kalman filters against non-Gaussian noise, demonstrating superior accuracy across multiple real-world datasets. More recently, *Javad* et al. [74] proposed an improved Extended Kalman Filter that adaptively adjusts the process and measurement noise covariance matrices using an interval Type-3 fuzzy set integrated with a covariance-matching technique, achieving superior estimation accuracy and robustness in ground-vehicle navigation. In a subsequent study, *Javad* et al. [75] introduced an adaptive Unscented Kalman Filter (UKF) combined with a Strong Tracking Filter (STF) and an interval type-3 fuzzy set to compensate for gyroscope bias and nonlinearities in attitude and heading reference systems, significantly improving stability under strong measurement uncertainty. These studies show that combining fuzzy inference with Kalman filter techniques improves robustness, adaptability, and estimation accuracy in nonlinear and uncertain systems. Building on previous advances, the current study combines an Autoregressive type-3 Fuzzy Logic (AR-T3FL) model with the Extended Kalman Filter (EKF) to improve lattice-constant prediction for perovskite and double perovskite materials, where structural uncertainty and noisy, limited data remain significant challenges.

This paper proposes a new optimized hybrid autoregressive Type-3 Fuzzy Logic System that combines the dynamic modeling capability of autoregressive structures with Type-3 fuzzy logic's excellent uncertainty-handling capabilities. The model's capacity to represent nonlinear correlations in high-dimensional compositional data is improved by adding an autoregressive formulation, which uses recursive propagation of fuzzy rules to describe internal relationships among input descriptors. Conceptually, this method is comparable to using autoregressive reasoning in non-temporal domains like feature sequences or spatial data, where the "temporal" index just denotes the order of characteristics or latent states rather than actual time. Type-3 fuzzy sets provide a third degree of uncertainty modeling to better reflect profound epistemic and stochastic ambiguity in complicated or nonlinear time se-

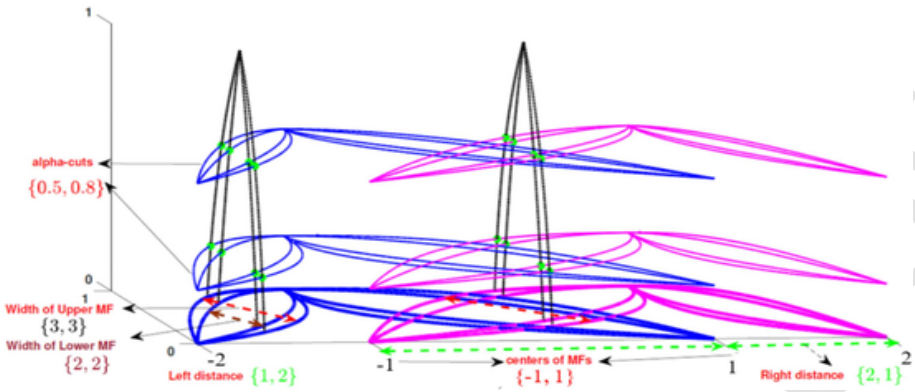

Fig. 7. Illustrative example of membership function design.

Table 3
Comparison of Evaluation Metrics for the Proposed and Conventional T3FLS Models.

Metrics	Conventional T3FLS Model			Proposed Model		
	First dataset [6]	Second dataset [5]	Third dataset [7]	First dataset [6]	Second dataset [5]	Third dataset [7]
MSE	0.0521	0.0533	0.0248	**$3.5628e^{-05}$**	**$3.4704e^{-05}$**	**$1.1719e^{-04}$**
RMSE	0.2282	0.2310	0.1574	**0.0060**	**0.0059**	**0.0125**
MAE	0.2145	0.1950	0.1067	**0.0043**	**0.0042**	**0.0080**
R^2	0.9657	0.9516	0.7591	**0.9999**	**0.9999**	**0.9982**

ries data. The extended kalman filter is used as an adaptive state estimator to improve the type 3 fuzzy membership functions and rule base parameters by minimizing estimate error covariance, resulting in more accurate and stable convergence. The incorporation of EKF into AR-T3FLS guarantees rapid learning, robustness to highly nonlinear input, and increased generalization performance. The proposed framework has great potential in predicting material physical characteristics, when data uncertainty and nonlinearity dominate.

The extended kalman filter and Autoregressive Type-3 Fuzzy Logic Systems (AR-T3FLS) provide a robust framework for modeling and prediction in highly uncertain environments. The AR model captures temporal relationships in time series data, whereas the Type-3 fuzzy logic system handles multi-level uncertainty in membership functions and fuzzy rules. The Type-3 system, in contrast to conventional fuzzy systems, uses a third-order fuzzy set to improve the expressiveness and adaptability of describing ambiguous and nonlinear data. EKF is an important online optimization method because it iteratively updates system parameters based on incoming observations using a prediction-correction process that accommodates nonlinearity. This synergy allows the AR-T3FLS to dynamically adapt to complicated data, resulting in higher predicted accuracy and resilience than traditional approaches.

Double perovskites, having the formula $A_2BB'X_6$, are complex crystal materials with great structural and chemical variety due to the presence of two distinct cations at the B-site. Conventional prediction models struggle to represent the complicated relationships between atomic radii, electronegativity, and bonding geometry. The proposed autoregressive type-3 fuzzy logic system optimized with the extended Kalman filter models uncertainty and nonlinear interactions in such materials to provide a robust solution. This method can reliably estimate double perovskite lattice constants and other structural characteristics even with little data. This is essential for expediting the discovery and design of next-generation functional materials with customized features for photovoltaics, catalysis, and electronics.

To assess the performance and the efficiency of our suggested model, we carried out a detailed comparative study with various recently published models [5–7]. These benchmark models, including machine learning-based techniques such as Support Vector Regression (SVR), Gaussian Process Regression (GPR), Artificial Neural Networks (ANNs), Ensemble Regression Trees (ERT), and Type 1 Fuzzy logic (T1FL), have demonstrated promising results in predicting lattice constants. However, our method consistently outperformed them in terms of prediction accuracy, robustness to limited data, and generalization to complex material classes such as double perovskites. Notably, our model achieved higher coefficient of determination and lower error margins across diverse datasets. These results demonstrate the superiority of our approach and its potential as a reliable predictive tool for complex materials science problems.

Finally, the main contributions of this study are:

- ✓ A novel AR–T3FLS–EKF predictive framework that combines autoregressive modeling, advanced fuzzy logic, and EKF-based learning for lattice constant estimation.
- ✓ Enhanced uncertainty modeling through Interval Type-3 fuzzy logic, enabling explicit handling of both epistemic and linguistic uncertainty.
- ✓ Robust and adaptive optimization using the Extended Kalman Filter, ensuring efficient convergence and resilience to measurement noise.
- ✓ Improved generalization with limited datasets, leveraging the autoregressive structure to propagate compositional dependencies.
- ✓ Comprehensive validation and comparative analysis demonstrating the superiority of the proposed model over conventional fuzzy and metaheuristic-based methods.

2. Dataset description and pre-processing

The perovskites typically follow the general formula ABO_3 or $A_2BB'X_6$, where 'A' and 'B' are cations, 'A' having a larger ionic radius than 'B' and 'X' represents small-radius anions such as halogens or oxygen. The ABO_3 structure is known as a simple perovskite, while $A_2BB'X_6$ denotes a double perovskite. Depending on whether the A-site cation is a metal ion or an organic molecule, simple perovskites can be classified as inorganic or hybrid organic–inorganic perovskites. In their ideal cubic structure, A-site cations occupy the cube's corners, B-site cations are located at the center, and the X-site anions sit at the center of each face [38]. However, not all ABX_3-type compounds actually adopt a perovskite crystal structure. Thus, a key challenge in the discovery and design of perovskites lies in efficiently determining whether a given ABX_3 compound will form a stable perovskite structure. A commonly used metric for this purpose is the Goldschmidt tolerance factor (t) [38],

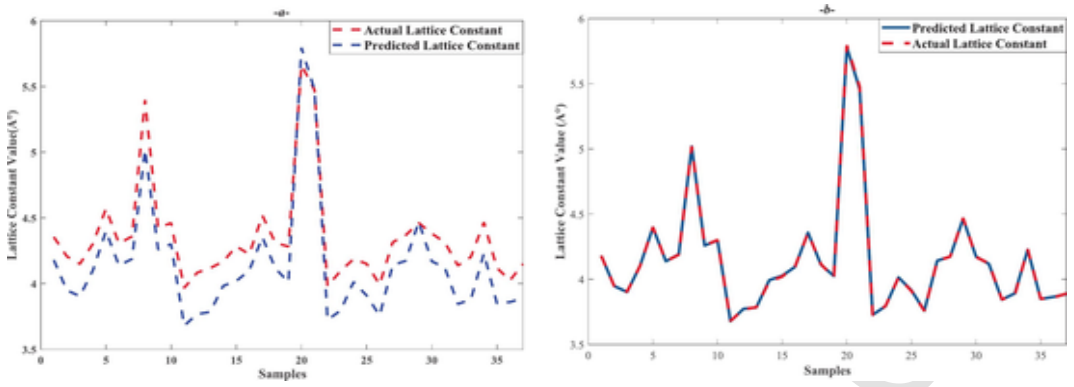

Fig. 8. Superposition of predicted and actual lattice constants for simple perovskite materials with twelve inputs: (a) conventional T3FLS model, (b) proposed model.

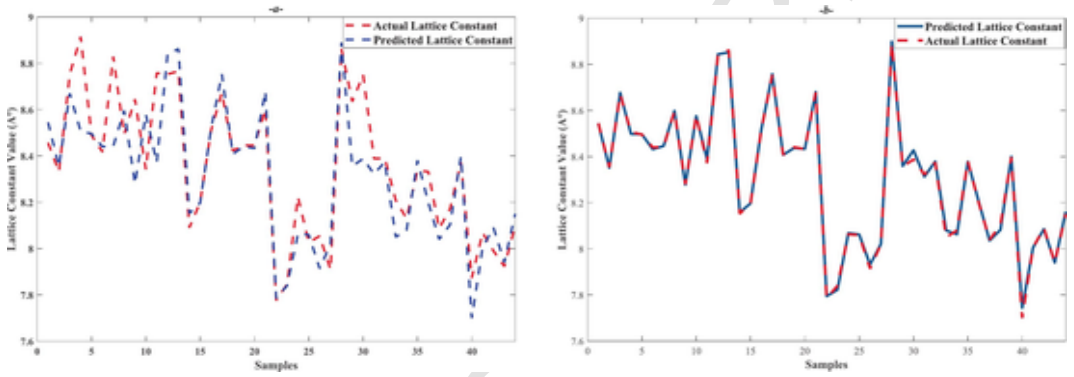

Fig. 9. Superposition of predicted and actual lattice constants for double perovskite materials: (a) conventional T3FLS model, (b) proposed model.

which assesses structural feasibility and phase stability. Nevertheless, as the diversity of perovskites grows, this factor alone has proven insufficient. To address this limitation, researchers have introduced new predictive methods. For example, Sun et al. [76] proposed a combined descriptor using both the tolerance and octahedral factors, achieving an accuracy of 90 %. Additionally, Bartel et al. [77] introduced an alternative tolerance factor (see Formula (2)) to enhance the prediction of perovskite formability of simple perovskite and double perovskite, defining when τ of the compounds less than 4.18 represents perovskite with 91 % accuracy.

$$t = \frac{r_A + r_X}{\sqrt{2}\left(r_B + r_X\right)} \tag{1}$$

$$\tau = \frac{r_X}{r_B} - n_A\left(n_A - \frac{\frac{r_A}{r_B}}{\ln\left(\frac{r_A}{r_B}\right)}\right) \tag{2}$$

where: r_A, r_B and r_X are ionic radii of A, B, and X respectively. n_A: is the oxidation state of A.

To thoroughly assess the effectiveness and generalization capability of our proposed AR-T3FS-EKF model, three different datasets were employed in the evaluation process. These datasets, chosen for their diversity and relevance, allow us to examine the robustness of our approach across varying data distributions and material characteristics. Additionally, to ensure a fair and consistent comparison, we benchmarked our model against several recent techniques using the same datasets and experimental settings [5–7].

The first dataset used to train and validate our model, comprising 122 unique ABO_3 perovskite compounds [6,39], this dataset contains a rich range of carefully selected descriptors, including ionic radii, electronegativity, atomic number, and density to capture the main chemical and structural factors that affect lattice constant parameter. This dataset supports perovskite structural modeling with low computational overhead. Our AR-T3FS-EKF approach's prediction accuracy and generalization are measured against it. This dataset models lattice constant with the following descriptors:

- ***Ionic Radii***: r_A for the A-site cation, r_B for the B-site transition metal, and r_X for the X-site ion, either a halide or oxygen.
- ***Density***: *DA* for the A-site element, *DB* for the B-site element, and *DX* for the X-site ion.
- ***Electronegativity***: *XA* for the A-site, *XB* for the B-site, and *XX* for the X-site ion.
- ***Atomic Number***: *ZA* for the A-site, *ZB* for the B-site, and *ZX* for the X-site ion.

The second dataset used in this study comprises 127 cubic and pseudo-cubic ABO_3 perovskite compounds, where A represents alkaline earth metals (e.g., Ca, Ba, Sr), B denotes transition metals (e.g., Fe, Ti, Ni), and X is an oxide or halide ion [5]. This dataset includes key features such as the six-fold effective ionic radii (r_A, r_B, r_X) of the constituent ions, the Goldschmidt tolerance factor (*t*) (see Formula (1)), and experimental lattice constants (LC in Å). These parameters are critical for evaluating the structural stability and predicting the lattice constants of perovskites. All data were compiled from previous experimental studies, providing a solid foundation for machine learning-based modeling and validation of perovskite structures [78,79].

The third dataset comprises 147 experimentally characterized cubic double perovskite oxides with the general formula $A_2BB'X_6$ [7]. The

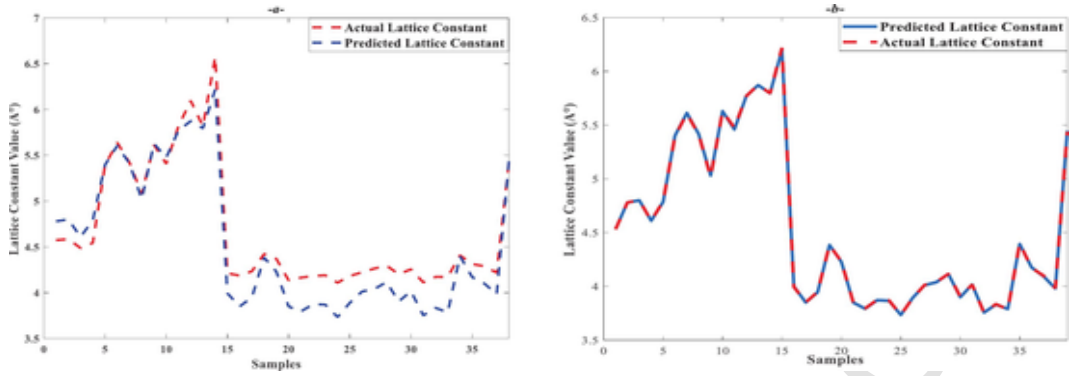

Fig. 10. Superposition of predicted and actual lattice constants for simple perovskite materials with four inputs: (a) conventional T3FLS model, (b) proposed model.

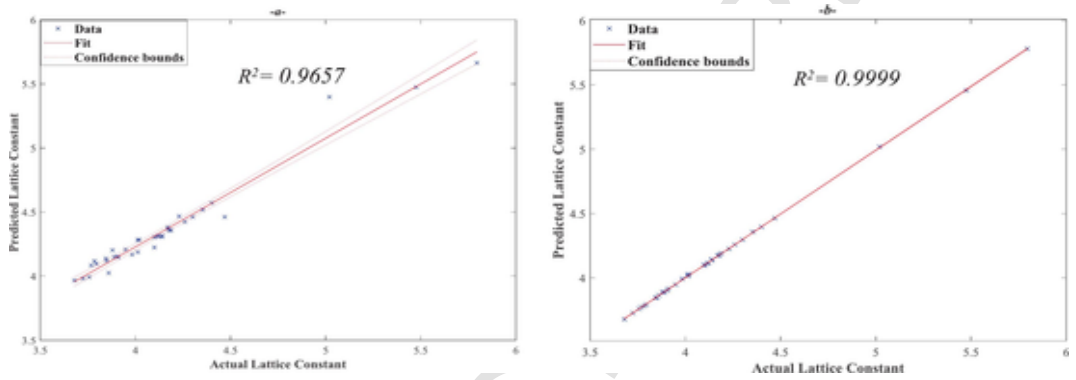

Fig. 11. Linear fit curves for simple perovskite materials with twelve inputs: (a) conventional T3FLS model, (b) proposed model.

materials included span a broad range of compositions, with A-site cations such as Ba, Ca, Pb, and Sr. The dataset features lattice constants varying from 7.700 Å to 8.890 Å. Descriptors used for modeling include ionic radii (r_A, r_B, $r_{B'}$), electronegativities (x_B, $x_{B'}$), and oxidation states (z_B), offering a detailed representation of the structural and electronic environments. This rich dataset provides a reliable benchmark for testing the generalizability and predictive performance of machine learning models in the context of complex perovskite materials.

Following data collection, one of the most important processes in developing regression-based machine learning models is data normalization. This procedure guarantees that all input characteristics are scaled to a similar range, preventing traits with higher numerical values from dominating the learning process. Normalization accelerates the convergence of several methods while improving overall model performance and stability. Without adequate normalization, regression models may give biased or inconsistent predictions, especially when the dataset includes variables with different units or scales. Thus, normalization is required to promote equitable learning and accurate findings. In this work, all data used for modeling and simulation were preprocessed and standardized to the [0,1] range using the following normalization formula:

$$\mathbf{Normalizeddata} = \frac{(\mathbf{data} - Min\,(\mathbf{data}))}{Max\,(\mathbf{data}) - Min\,(\mathbf{data})} \tag{3}$$

3. Autoregressive model

The Autoregressive model is a basic time-series modeling method that expresses a variable's current value as a linear combination of its prior values plus a stochastic error term. AR(p) is an autoregressive model that predicts the present using the past *p* observations to capture temporal correlations in the data. The model parameters define each lagged value's effect, whereas the error term compensates for random fluctuations not explained by prior values. The AR model is employed in stationary process forecasting, signal processing, and system identification because to its simplicity and efficacy.

Mathematically, autoregressive model of order *p*, denoted as AR(*p*) and can be expressed as:

$$X_t = c + a_1 X_{t-1} + a_2 X_{t-2} + \cdots + a_p X_{t-p} + \varepsilon_t; \tag{4}$$

where: X_t is the value at time *t*, c is a constant, $a_1, a_2, \cdots, a_p$ are the model parameters, $X_{t-1}, X_{t-2}, \cdots, X_{t-p}$ are the previous values, and ε_t represents the error a time *t*.

In the proposed AR–T3FLS-EKF model, the autoregressive formulation is not meant to physically reflect temporal variation, even if the lattice constant is a static compositional characteristic. Rather, it functions as a framework for mathematics that captures recursive relationship and ordered dependencies among compositional descriptors. Features like the tolerance factor, electronegativity, and ionic radius frequently show progressive and connected impacts on the lattice constant in materials datasets. To improve the fuzzy system's ability to learn intricate nonlinear mappings from limited and noisy data, the autoregressive component treats these dependencies similarly to temporal correlations, allowing information to spread over consecutive feature states. This formulation offers a more flexible representation of interdependent compositional impacts on the lattice constant, extending the expressive capacity of the fuzzy model beyond static mapping.

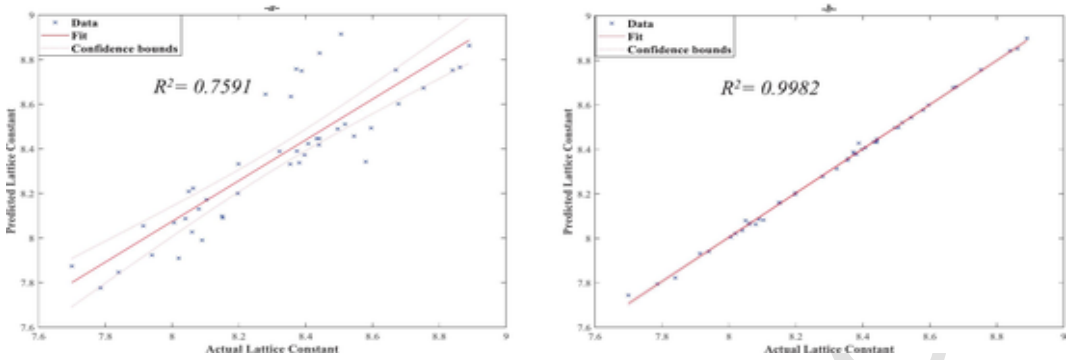

Fig. 12. Linear fit curves for double perovskite materials: (a) conventional T3FLS model, (b) proposed model.

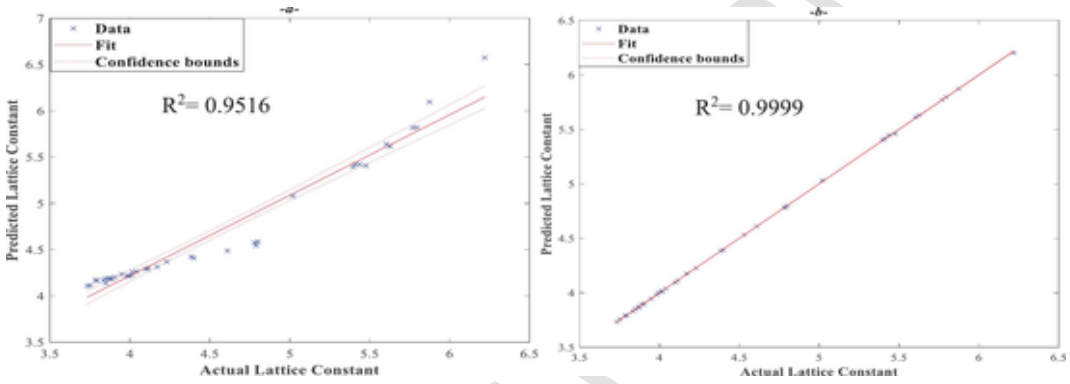

Fig. 13. Linear fit curves for simple perovskite materials with four inputs: (a) Conventional T3FLS model; (b) proposed model.

4. Type 3 fuzzy logic system

Type-3 Fuzzy Logic is an advanced extension of classical Type-1 and Type-2 fuzzy logic systems, designed to model higher levels of uncertainty in decision-making, inference, and modeling tasks. Each level in the hierarchy of fuzzy logic aims to handle more complex forms of imprecision:

- ✓ ***Type-1 fuzzy logic:*** deals with precise membership functions;
- ✓ ***Type-2 fuzzy logic:*** allows the membership degree itself to be fuzzy, often represented as a fuzzy set of values (e.g., an interval);
- ✓ ***Type-3 fuzzy logic:*** takes this one step further by allowing the secondary membership functions in Type-2 fuzzy sets to themselves be fuzzy sets, effectively creating "fuzzy membership of fuzzy memberships".

Fig. 1 shows the output of the type-3 Fuzzy Logic model, which incorporates higher-order uncertainty. Figs. 2 and 3 show the offered MFs with some vertical and horizontal cuts. In comparing the designed MF shown in Fig. 4 to conventional general type-2 MF displayed in Fig. 5, it is seen that the upper and lower limits of the foot of uncertainty (FOU) in the employed MF are not known values, but they are interval type-1 MFs. This additional degree of freedom allows the suggested FLS to tolerate a larger amount of uncertainty. The specified membership function was used owing to its capacity to manage high-order uncertainty and non-symmetric distributions. Unlike Gaussian membership functions that assume symmetric uncertainty, the employed MF allows for flexible FOU modeling, enhancing robustness under noisy or inaccurate data.

The initial step in the process involves obtaining the inputs (data collection step). The inputs are represented by $x_1, x_2, \cdots x_n$, where each x_i denotes a specific feature relevant to the system. Each x_i input is associated with a set of membership functions $\widetilde{M}_i^j(x_i)$, where i is the i^{th} input, and j is the j^{th} membership function of i^{th} input. The type-3 fuzzy logic system (T3FLS) introduces horizontal slices representing the secondary membership α_k. For each slice, we consider four principal membership values: the upper and lower bounds on the right side, denoted as $\overline{P}_{i,r,\alpha_k}$ and $\underline{P}_{i,r,\alpha_k}$, and the corresponding bounds on the left side, denoted as $\overline{P}_{i,l,\alpha_k}$ and $\underline{P}_{i,l,\alpha_k}$. These boundaries reflect the uncertainty in both the membership grade and its relative reliability. The firing degrees are calculated for the membership function as following [80]:where: ${}^{c}\widetilde{M}_i^j$: is the center of $\widetilde{M}_i^j$; $\underline{\vartheta}_{\widetilde{M}_i^j}$ and $\overline{\vartheta}_{\widetilde{M}_i^j}$: are the widths of the left and right sides of $\widetilde{M}_i^j$; α_k: is the value of the horizontal slice; Δ_r and Δ_l: are the widths of the membership functions.

The rule firings are determined based on the upper and lower boundary memberships of the membership functions $\widetilde{M}_i^j$, as follows:

$$\overline{z}_{r,\alpha_k} = \overline{s}_{\widetilde{M}_1^{h_1}|r,\ \alpha_k}(x_1).\overline{s}_{\widetilde{M}_2^{h_2}|r,\ \alpha_k}(x_2).\ldots.\overline{s}_{\widetilde{M}_n^{h_n}|r,\ \alpha_k}(x_n) \tag{9}$$

$$\underline{z}_{r,\alpha_k} = \underline{s}_{\widetilde{M}_1^{h_1}|r,\ \alpha_k}(x_1).\underline{s}_{\widetilde{M}_2^{h_2}|r,\ \alpha_k}(x_2).\ldots.\underline{s}_{\widetilde{M}_n^{h_n}|r,\ \alpha_k}(x_n) \tag{10}$$

$$\overline{z}_{l,\alpha_k} = \overline{s}_{\widetilde{M}_1^{h_1}|l,\ \alpha_k}(x_1).\overline{s}_{\widetilde{M}_2^{h_2}|l,\ \alpha_k}(x_2).\ldots.\overline{s}_{\widetilde{M}_n^{h_n}|l,\ \alpha_k}(x_n) \tag{11}$$

$$\underline{z}_{l,\alpha_k} = \underline{s}_{\widetilde{M}_1^{h_1}|l,\ \alpha_k}(x_1).\underline{s}_{\widetilde{M}_2^{h_2}|l,\ \alpha_k}(x_2).\ldots.\underline{s}_{\widetilde{M}_n^{h_n}|l,\ \alpha_k}(x_n) \tag{12}$$

$\widetilde{M}_i^{h_i}$ represent the h_i^{th} membership function for input x_i, the h^{th} rule is defined as:

if $x_1$is $\widetilde{M}_i^{h_1}$, …, ***and***, … x_n is $\widetilde{M}_i^{h_n}$, ***then.***

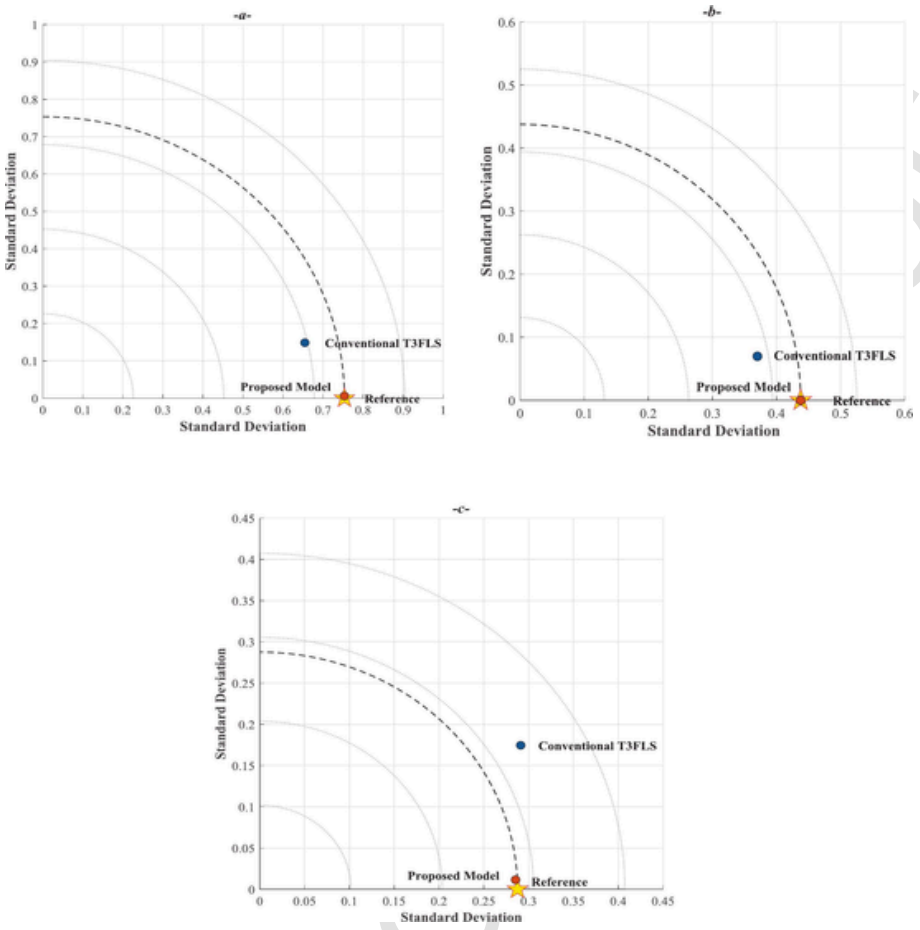

Fig. 14. Taylor Diagram for, (a) dataset 1 [5], (b) dataset 2 [6], (c) dataset 3 [7].

Table 4
Performance Comparison of the Proposed AR-T3FLS-EKF Model and Benchmark Methods for Lattice Constant Prediction of Simple Perovskites.

Model	*RMSE*	R^2	*MAE*
GPR Model [6]	0.0371	99 %	0.2798
Ensemble Model [6]	0.0555	99 %	0.03676
Neural Network Model [6]	0.0398	99 %	0.0309
SVM [6]	0.0454	99 %	0.0338
Proposed Model	**0.0060**	**99.99 %**	**0.0043**

$$y_h \in \left[\left[\underline{\Psi}_{l,h}, \underline{\Psi}_{r,h}\right] \quad \left[\overline{\Psi}_{l,h}, \overline{\Psi}_{r,h}\right]\right], \quad h = 1, \ldots, M, \tag{13}$$

where $\underline{\Psi}_{l,h}, \underline{\Psi}_{r,h}$, $\overline{\Psi}_{l,h}$ and $\overline{\Psi}_{r,h}$ are the consequent parameters.

Finally, the output of the type 3 fuzzy logic system is expressed as following [80]:

$$\widehat{f} = \frac{\sum_{k=1}^{K}\left(\overline{\phi}_k + \underline{\phi}_k\right)\alpha_k}{\sum_{k=1}^{K}\alpha_k} \tag{14}$$

where:

$$\overline{\phi}_k = \frac{\sum_{h=1}^{M}\left(\underline{z}^h_{r,\alpha_k}\overline{\Psi}^h_{r,k} + \underline{z}^h_{l,\alpha_k}\underline{\Psi}^h_{l,k}\right)}{\sum_{h=1}^{M}\underline{z}^h_{r,\alpha_k} + \underline{z}^h_{l,\alpha_k}} \tag{15}$$

$$\underline{\phi}_k = \frac{\sum_{h=1}^{M}\left(\underline{z}^h_{r,\alpha_k}\underline{\Psi}^h_{r,k} + \overline{z}^h_{l,\alpha_k}\overline{\Psi}^h_{l,k}\right)}{\sum_{h=1}^{M}\underline{z}^h_{r,\alpha_k} + \overline{z}^h_{l,\alpha_k}} \tag{16}$$

The adopted fuzzy inference approach generates rule outputs as mathematical functions with direct crisp values, removing the necessity for defuzzification in Mamdani systems. Table 1 shows a comparison of the Mamdani and suggested inference systems across many performance metrics, which supports the selected strategy.

5. Extended Klaman filter

The Extended Kalman Filter (EKF) is an advanced variant of the Kalman filter designed to estimate the state of systems with nonlinear dynamics by incorporating noisy measurements and a mathematical model of the system [68]. The EKF addresses nonlinearity by linearizing the state transition and measurement models around the current estimate using a Taylor series expansion and the Jacobian matrix. For a discrete and nonlinear system $x_{k+1} = f\left(x_k, w_k\right)$ and its nonlinear obser-

Table 5
Performance Comparison of the Proposed AR-T3FLS-EKF Model and Benchmark Methods for Lattice Constant Prediction of Double Perovskites.

Model	*RMSE*	R^2	*MAE*
GPR Model [7]	0.024	99.62 %	0.016
MLR Model [7]	0.048	99.43 %	0.038
ANN Model [7]	0.050	98.52 %	0.037
Proposed Model	**0.0125**	**99.82 %**	**0.0080**

vation $y_k = g\left(x_k, v_k\right)$, the extended Kalman filter equations can be given as following:

$$\hat{x}_{k/k+1} = f\left(\hat{x}_{k-1/k-1}, 0\right); \tag{17}$$

$$P_{k/k+1} = \boldsymbol{A_k} P_{k-1/k-1} \boldsymbol{A_K^T} + \boldsymbol{F_k Q_k F_k^T}; \tag{18}$$

$$\hat{x}_{k/k} = \hat{x}_{k/k-1} + K_k\left[y_k - g\left(\hat{x}_{k/k-1}, 0\right)\right]; \tag{19}$$

$$K_k = P_{k/k-1} \boldsymbol{C_K^T}\left[\boldsymbol{C_k} P_{k/k-1} \boldsymbol{C_k^T} + \boldsymbol{G_k^T}\right]^{-1} \tag{20}$$

$$P_{k/k} = P_{k/k-1} - K_k \boldsymbol{C_k} P_{k/k-1} \tag{21}$$

where $\hat{x}_{k/k-1}$ represents the estimate of the state vector x_k at the instant k, based on the observations y_1 to y_{k-1} and $\hat{x}_{k/k}$ represents the estimate of the state vector x_k at the instant k, based on the observations y_1 to y_k. $P_{k/k-1}$represents the estimation of the a priori error covariance matrix and $P_{k/k}$ is the estimation of the a posteriori covariance matrix. $\boldsymbol{R}$ and $\boldsymbol{Q}$ are the measurement and process covariance matrices respectively. K_k is the Kalman gain and $\boldsymbol{A_k}$,$\boldsymbol{F_k}$,$\boldsymbol{C_k}$,$\boldsymbol{G_k}$ are the jacobian matrices.

For optimization purposes, the extended Kalman filter can be employed as an adaptive estimation technique that iteratively updates model parameters to minimize prediction error. The EKF sees the parameters that need to be optimized as parts of the system state vector. This lets it keep track of how they change over time. The EKF uses the Jacobian matrix to linearize the nonlinear system dynamics and measurement functions around the present estimate. It then predicts the next parameter values and their uncertainty and corrects them using new observations and the Kalman gain. This iterative method successfully merges existing knowledge with new data, facilitating rapid convergence and resilience against measurement uncertainty [68,81–83].

6. Evaluation metrics

The proposed Model performance was evaluated using three standard regression metrics: the coefficient of determination ($R2$), root mean square error (*RMSE*), and mean absolute error (*MAE*). *MAE* (Eq. (22)) quantifies the average prediction error, whereas *RMSE* (Eq. (23)) penalizes larger deviations, making it sensitive to outliers. R^2 (Eq. (24)) indicates the proportion of variance explained by the model. Lower *MAE* and *RMSE* values denote better predictive accuracy, expressed in Å in this study. These metrics are widely applied in machine learning and statistical regression analysis.

$$MAE = \frac{1}{n}\sum_{i=1}^{n}\left|y_i - \hat{y}_i\right| \tag{22}$$

$$RMSE = \sqrt{\frac{1}{n}\sum_{i=1}^{n}\left(y_i - \hat{y}_i\right)^2} \tag{23}$$

$$R^2 = 1 - \left(\frac{\sum_{i=1}^{n}\left(y_i - \hat{y}_i\right)^2}{\sum_{i=1}^{n}\left(y_i - \bar{y}_i\right)^2}\right) \tag{24}$$

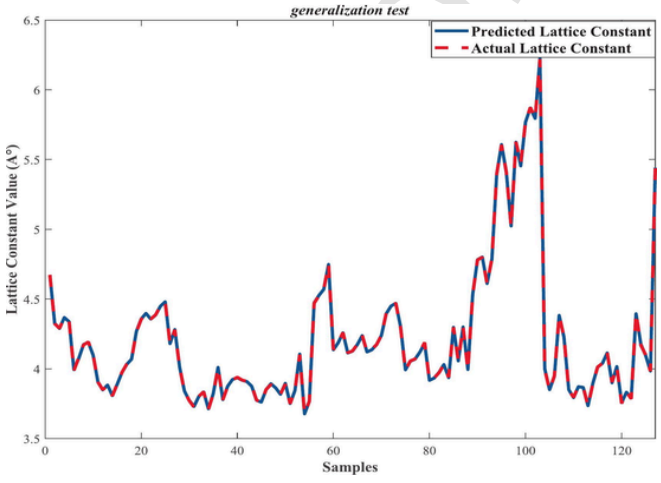

Fig. 15. Actual vs. Predicted Lattice Constants for Simple Perovskites in the Generalization Test.

7. Methodology

In this study, we introduce an Autoregressive Type-3 Fuzzy Logic (AR-T3FL) model specifically designed for predicting the lattice constant of perovskite materials. The proposed model integrates the temporal dependency structure of the autoregressive approach with the advanced uncertainty-handling capability of type-3 fuzzy logic, enabling accurate modeling of complex and imprecise relationships between structural parameters and lattice constants. In the AR-T3FL framework, the lagged lattice constant values and the error between the actual lattice constant value and the predicted one are incorporated as autoregressive inputs, while material descriptors, such as ionic radii, density, electronegativity, and tolerance are processed through a type-3 fuzzy inference system. The latter employs horizontal slices and secondary membership functions to capture higher-order uncertainties inherent in experimental and simulated data. Model parameters, including membership function centers, boundaries and rule weights, are optimized using an extended kalman filter to enhance prediction accuracy. This hybrid design not only addresses nonlinearity and variability in material datasets but also ensures better generalization to diverse perovskite and double perovskite compositions. The proposed approach aims to provide a robust and interpretable predictive tool to accelerate the design of novel perovskite-based materials.

$$X_t = \mathbf{C} + a_1 X_{t-1} + a_2 X_{t-2} + \cdots + a_p X_{t-p} + \varepsilon_t; \tag{22}$$

where: X_t: Is the predicted Lattice Constant Value. $\mathbf{C}$: is a vector of Perovskite Lattice Constant features. $X_{t-1}, X_{t-2}, \cdots, X_{t-p}$: are the lagged values of the predicted lattice constant. ε_t: is the error between the actual and predicted values of the lattice constant.

The structure of the proposed scheme is given in Fig. 6; where the boxes showing delay refer to the previous value of the predicted lattice constant. The task now is to adjust online the parameters of the proposed autoregressive type-3 fuzzy logic model using the extended Kalman filter until the error between the actual lattice constant value and the output of the proposed model reaches its smallest value. The parameters of type-3 fuzzy logic system to be optimized using the optimization process are the center, the widths of the type-3 membership functions and the value of the horizontal slice ($^{c}\widetilde{M}_i^j$, $\underline{\vartheta}_{\widetilde{M}_i^j}$, $\overline{\vartheta}_{\widetilde{M}_i^j}$, and Δ_l) (for more details, refer to the Section 4).

For each input variable, three membership functions (MFs) are defined, denoted as $\widetilde{M}_i^1$, $\widetilde{M}_i^2$ and $\widetilde{M}_i^3$ where i represents the i^{th} input. The datasets were normalized to ensure that all input features are scaled within a comparable range, preventing variables with larger magnitudes from dominating the learning process. Consequently, all input membership functions share the same shape and initial parameters,

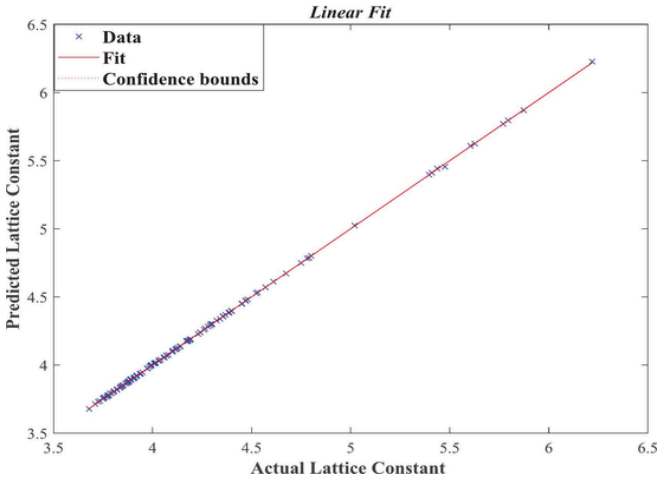

Fig. 16. Linear fit between actual and predicted lattice constants for simple perovskites in the generalization test.

Table 6
Generalization Performance Comparison of the Proposed AR-T3FLS-EKF Model and Benchmark Methods.

Model	Metrics			
	MSE	*RMSE*	*MAE*	R^2
ANN-PSO [5]	$1.3459e^{-4}$	0.0108	0.0085	0.9997
ANN-IWO [5]	$1.6776e^{-04}$	0.0130	0.0112	0.9981
ANN-ICA [5]	$5.330e^{-04}$	0.0235	0.0198	0.9944
Fuzzy-PSO [5]	$5.6568e^{-06}$	0.0024	0.0019	0.9989
Proposed Model	$\mathbf{1.4400e^{-06}}$	**0.0012**	**0.0015**	**0.9999**

providing consistent fuzzy partitioning across the inputs. The initial parameters of the membership functions are summarized in Table 2, and the corresponding configuration is illustrated in Fig. 7.

To optimize the performance of the proposed autoregressive Type-3 fuzzy logic system for lattice constant prediction, the extended kalman filter EKF is employed to adaptively tune its key parameters. Specifically, the parameters subject to optimization include the centers, widths, and slice parameters of the Type-3 membership functions. The EKF is particularly well-suited for this task due to its ability to estimate parameters in nonlinear and uncertain environments by recursively updating their values based on incoming data. The tuning process begins with an initial hypothesis for each parameter, which serves as the prior state estimate. At each iteration, the autoregressive model output is compared with the actual lattice constant, and the prediction error is computed. This error, along with the system's Jacobian matrices, is used by the EKF to update the parameter estimates in a way that minimizes the mean-square prediction error. By iteratively adjusting the membership function parameters, the EKF ensures that the fuzzy inference system accurately captures the complex nonlinear relationships inherent in perovskite material properties, thereby improving generalization and predictive accuracy.

The followed methodology for Parameters Tuning using Extended Kalman filter is:

- The first step involves defining the state vector, which encompasses all the tunable parameters of the proposed T3FLS, including the membership function centers, widths, and horizontal slice parameters:

$$\mathbf{x} = \begin{bmatrix} c_{\tilde{M}_i^j} & \underline{\vartheta}_{\tilde{M}_i^j} & \bar{\vartheta}_{\tilde{M}_i^j} & \underline{\vartheta}_{\tilde{M}_i^j} & \Delta_r & \Delta_l \end{bmatrix}^T \tag{23}$$

- The second step is to establish the state transition model, under the assumption that the parameters evolve according to:

$$x_k = x_{k-1} + w_{k-1} \tag{24}$$

where w_{k-1} represents the process noise.

- The third step is to formulate the measurement model, in which the EKF measurement equation maps the parameters to the predicted output of the T3FLS:

$$y_k = f\left(u_k, x_k\right) + v_k; \tag{25}$$

where $f(.)$ is the forward computation of our proposed autoregressive T3FLS given input u_k and v_k is the measurement noise. In the initial assessment phase, the measurement noise term (v_k) was set to zero. This assumption was introduced deliberately to simplify the problem and to isolate the role of structural uncertainty modeled by the autoregressive type-3 fuzzy logic component. Since the dataset used in this study did not incorporate experimental variability, this assumption allows us to focus on the theoretical properties of the proposed AR-T3FLS-EKF framework. In the second assessment phase, the model was updated to include a realistic, non-zero v_k, modeled as Gaussian noise with empirically estimated covariance measurement noise $\boldsymbol{R}$.

Following these steps, the extended Kalman filter is initialized as follows:

✓ Set initial parameter estimates x_0;
✓ Initialize the error covariance matrix $\mathbf{P_0}$.

- The final step is to implement the extended Kalman filter process as follows:

1. Predict the next parameter estimates:

$$\hat{x}_{k/k-1} = \hat{x}_{k-1} \tag{26}$$
$$P_{k/k-1} = P_{k-1} + \boldsymbol{Q} \tag{27}$$

The process noise covariance matrix $\boldsymbol{Q}$ was estimated through empirical tuning. Since $\boldsymbol{Q}$ controls the extent to which the extended Kalman filter adapts to parameter variations, an inappropriate value may lead either to excessive sensitivity or to filter divergence. To determine an optimal setting, several candidate values of $\boldsymbol{Q}$ were evaluated, and the configuration that minimized the root mean square error (*RMSE*) was selected. This empirical tuning strategy allows balancing between adaptability and numerical stability.

2. Compute the Jacobian matrix: Linearize the nonlinear measurement f (.) around the current parameter estimate to get the measurement Jacobian matrix $\mathbf{H_k}$:

$$\boldsymbol{H_k} = \left.\frac{\partial f}{\partial x}\right|_{\hat{x}_{k/k-1}} \tag{28}$$

3. Compute the Kalman gain:

$$K_k = P_{k/k-1}\boldsymbol{H_k^T}\left(\boldsymbol{H_k}P_{k/k-1}\boldsymbol{H_k^T} + \boldsymbol{R}\right)^{-1} \tag{29}$$

4. Update the proposed model parameters:

$$\hat{x}_k = \hat{x}_{k/k-1} + K_k\left(y_k - f\left(u_k, \hat{x}_{k/k-1}\right)\right) \tag{30}$$

Table 7
Summary of 5-fold cross-validation showing the best and worst performance values of the proposed AR–T3FLS–EKF model in terms of R^2 and MSE.

	R^2		MSE	
	Best	Worst	Best	Worst
The first dataset	0.9999	0.9973	$3.7533e^{-05}$	$4.9356\ e^{-05}$
The second dataset	0.9999	0.9970	$3.5532e^{-05}$	$3.9345e^{-05}$
The Third dataset	0.9983	0.9962	$1.1622e^{-04}$	$2.1719e^{-04}$

5. Update error covariance:

$$P_k = P_{k/k-1} - K_k \boldsymbol{H_k} P_{k/k-1} \tag{31}$$

This procedure keeps on until the performance criteria reaches its lowest value, which means that the settings have been tuned to their best.

8. Results and discussion

To show how well the suggested autoregressive type-3 fuzzy logic system works when combined with the extended Kalman filter, the evaluation process is performed in two phases:

1- In the first phase the used data sets are considered clean (*idealized conditions*); to isolate the contribution of structural uncertainty captured by the fuzzy logic component and to evaluate the theoretical performance of the proposed AR-T3FL-EKF framework under idealized conditions. This phase is divided into three steps. Initially, the efficacy of the suggested model is evaluated in comparison to a standard Type-3 fuzzy logic system devoid of autoregressive integration, aiming to delineate and measure the advantages of the proposed enhancements. Next, the model's ability to make accurate predictions and its strength are tested against a number of contemporary state-of-the-art methods [5–7] using several assessment criteria, including *MSE*, *RMSE*, *MAE*, and R^2. Finally, the model's ability to generalize is tested using separate datasets. This makes sure that its ability to predict goes beyond the training settings. This systematic review gives a full and fair picture of how well the suggested technique works, both in terms of accuracy and generalization.
2- In the second phase, the model was evaluated under realistic conditions by introducing Gaussian noise with different variance levels to the used datasets. A sensitivity analysis of the extended kalman filter was also conducted to assess its performance under different measurement and process noise values. This study highlights how changes in noise characteristics impact the filter's accuracy and stability under realistic conditions.

In this investigation, the available datasets were randomly partitioned into two subgroups to guarantee an impartial assessment of the proposed model. In particular, 70 % of the data was set aside for training, which let the model understand the underlying patterns, and the other 30 % was set aside for testing to assess its predictive performance. This random partitioning lowers the chance of overfitting and makes sure that the evaluation measures show how well the model can generalize.

8.1. Phase 1: Assessment under idealized conditions

The initial step of the analysis emphasizes a direct juxtaposition between the suggested autoregressive type-3 fuzzy Logic system and the traditional type-3 fuzzy logic methodology. To make sure the evaluation is fair, both models are trained and evaluated under the same conditions, using the same datasets and preprocessing methods. For each scenario, performance measures like *RMSE*, *MAE*, and R^2 are calculated (Table 3), showing the quantitative improvements that come from combining the autoregressive structure with EKF-based parameter tuning. This comparison shows clearly how the suggested strategy improves the accuracy and stability of predictions.

The comparative performance of the suggested optimized autoregressive type-3 fuzzy logic system (AR-T3FLS-EKF) and the traditional T3FLS during the test phase is shown in Figs. 8, 9, and 10. In order to ensure the robustness of the analysis across various crystal structures and input features, three different datasets were used in this evaluation: the first corresponded to a simple perovskite materials [6] with 12 input features (r_A, r_B, r_X, *XB, XX, ZA, ZB, ZX, DA, DB*, and *DX*); the second to a double perovskite materials [7]; and the third to a simple perovskite with four inputs (r_A, r_B, r_X, and t) [5]. These graphs allow for a direct visual evaluation of prediction accuracy by superimposing the actual lattice constant values with the predicted outputs of both models. The output of the suggested model more closely resembles the actual values, indicating that it is better able to represent the system's fundamental dynamics. This visual inspection unequivocally shows a decrease in prediction error when compared to the standard T3FLS, confirming the efficacy of the suggested technique.

Figs. 11–13 show the linear fit curves for the prediction results achieved using both the suggested model and the conventional T3FLS. The fit lines are constructed for three datasets: one for simple perovskite materials with 12 inputs, the other for double perovskite materials, and the third for simple perovskite materials with 4 inputs. In each example, the predicted lattice constants are compared to the reference values, and a least-squares regression line is fitted. The linear fit curves provide additional evidence that the proposed model outperforms the conventional T3FLS. For both the single and double perovskite datasets, the proposed model's fit lines have slopes and intercepts that are closer to ideal values, suggesting a better agreement between anticipated and actual lattice constants. Furthermore, the coefficient of determination R^2 from linear regression is consistently better for the proposed model, indicating lower residual variance and increased predictive reliability. These results show that the suggested strategy not only reduces prediction errors but also achieves a nearly perfect linear connection with the target values, indicating model correctness and resilience.

Taylor diagram (Fig. 14) depicts the standard deviation for the assessed models compared to the reference experimental data. The sug-

Table 8
Sensitivity analysis of the Extended Kalman Filter performance under different process (***Q***) and measurement (***R***) noise covariance values for Gaussian noise with standard deviation of 0.01 Å.

Measurement covariance noise ***R***	Process covariance noise ***Q***	Evaluation Results for the first dataset [6]			Evaluation Results for the second dataset [5]		
		RMSE	MSE	MAE	RMSE	MSE	MAE
R = 1.00E−03	***Q = 1.00E−03***	0.0161	2.580e−04	0.0090	0.0596	0.0036	0.0473
	Q = 1.00E−06	**0.0016**	**2.622e−06**	**0.0011**	**0.0011**	**1.167e−06**	**8.355e−04**
	Q = 1.00E−09	0.0061	3.781e−05	0.0048	0.0053	2.792e−05	0.0040
R = 1.00E−04	***Q = 1.00E−03***	Diverge					
	Q = 1.00E−06	**0.0014**	**1.896e−06**	**9.861e−04**	**0.0025**	**6.3204e−06**	**0.0016**
	Q = 1.00E−09	0.0036	1.262e−05	0.0027	*0.0034*	*1.123e−05*	*0.0026*

Table 9
Sensitivity analysis of the Extended Kalman Filter performance under different process (***Q***) and measurement (***R***) noise covariance values for Gaussian noise with standard deviation of 0.05 Å.

Measurement covariance noise ***R***	Process covariance noise ***Q***	Evaluation Metrics for the first dataset [6]			Evaluation Metrics for the second dataset [5]		
		RMSE	MSE	MAE	RMSE	MSE	MAE
R = 1.00E–03	***Q = 1.00E–03***	0.2263	0.1534	0.1534	0.0714	0.0051	0.0580
	Q = 1.00E–06	**0.0025**	**6.474e–06**	**0.0018**	**0.0023**	**5.214e–06**	**0.0016**
	Q = 1.00E–09	0.0092	8.411E–05	0.0071	0.0084	7.062e–05	0.0065
R = 1.00E–04	***Q = 1.00E–03***	diverge					
	Q = 1.00E–06	**0.0043**	**1.834e–05**	**0.0027**	**0.0031**	**9.619e–06**	**0.0022**
	Q = 1.00E–09	0.0064	4.048e–05	0.0042	0.0094	8.826e–05	0.0059

gested autoregressive type 3 fuzzy logic-based extended Kalman filter is closest to the reference point, suggesting a near-perfect correlation and a standard deviation that is closely related to the observed values. This closeness represents both great prediction accuracy and stability. In contrast, traditional type 3 fuzzy logic is placed further away from the reference point, resulting in reduced correlation or mismatched variability. These findings demonstrate that the suggested model not only maintains the variety of the real lattice constants, but also minimizes prediction error.

In the second step of assessment, the proposed AR-T3FLS-EKF model is compared to a number of previously published benchmark approaches for lattice constant prediction [6,7]. This comparison employs a variety of performance indicators, including the coefficient of determination (R^2), root mean square error (*RMSE*), and mean absolute error (*MAE*), to give a complete evaluation of prediction accuracy and error distribution. The trials are carried out on both the same simple and double perovskite datasets to enable a fair and uniform assessment. The numerical results presented in Tables 4 and 5, clearly show that the proposed model outperforms all benchmark approaches across all measures, demonstrating that it is better able to describe the complicated interactions regulating lattice constants in perovskites. The comparative study shows that the suggested model consistently outperforms recently published benchmark approaches in all assessment measures. Its better accuracy in predicting lattice constants, together with reduced error rates, demonstrates the suggested approach's suitability for both simple and double perovskite datasets. These results demonstrate that combining autoregressive modeling with type-3 fuzzy logic improves the model's capacity to reflect the complicated nonlinear interactions seen in perovskite materials.

The third assessment step, known as the generalization test, looks at how well the suggested autoregressive Type-3 fuzzy logic model can predict outcomes when applied to data that hasn't been seen before. The basic perovskite dataset [6] was the only dataset used in this experiment to train the model. New samples taken from the same material family but not utilized for training [5] were then used to test the model. This configuration guarantees that the assessment just assesses the model's resilience and flexibility, not its capacity to memorize training data.

Fig. 15 shows how the actual lattice constant values and the predicted values by the proposed autoregressive type-3 fuzzy logic system overlap throughout the generalization test. This figure makes it evident that the two curves are quite close to each other, with just a small amount of difference between the test samples. This tight agreement shows that the model can reliably represent the fundamental structural connections of perovskite materials, even when it is predicting data that it has never seen before. The close match between the predicted and actual values shows that the suggested method is strong and dependable in real-world prediction situations.

Fig. 16 shows the linear fit curve between the actual and predicted lattice constants. This gives a quantitative and visual inspection how accurate the predictions are. The curve demonstrates that the predicted values are quite near to the actual line, with only small differences. This excellent alignment shows that the model maintains high predictive accuracy even for data outside the training set, highlighting its strong generalization capability and reliability in practical applications.

The suggested scheme's generalization performance is quantitatively evaluated using conventional regression metrics and compared to results obtained from ANN and Fuzzy logic type 1 approaches improved using numerous optimization algorithms (PSO, IWO, and ICA) described in a previous work [5]. The numerical results are listed in Table 6. These results show that the suggested model has improved generalization capacity, with lower error values and stronger correlation coefficients across test situations. The proposed AR–T3FLS–EKF framework distinguishes itself from existing machine learning and fuzzy hybrid models through the combined use of Autoregressive Type-3 Fuzzy Logic and Extended Kalman Filter based optimization. While previous studies have relied on models such as SVR, GPR, ANN, or Type-2 fuzzy systems, the introduction of the type-3 fuzzy logic system enhances the model's capacity to explicitly represent both epistemic and linguistic uncertainties via its footprint of uncertainty (FOU). This richer representation provides superior adaptability and interpretability, particularly when dealing with limited or noisy compositional data. Furthermore, the integration of the EKF as an optimization mechanism offers an adaptive, gradient-informed, and noise-aware learning process. Unlike population-based metaheuristic algorithms (PSO, IWO, ICA), which depend on random exploration and are sensitive to parameter tuning, the EKF ensures deterministic convergence, efficient computation, and robust parameter adaptation under uncertainty. The synergy between the Type-3 fuzzy representation and EKF-based optimization thus enhances both the predictive reliability and generalization capability of the proposed model.

To further evaluate the generalization capability of the proposed autoregressive Type-3 fuzzy logic–based EKF model and to avoid potential overfitting, a 5-fold cross-validation procedure was conducted. The dataset was randomly divided into five equal subsets. In each iteration, four subsets were used for training while the remaining subset served for validation. This process was repeated five times so that each fold was used once for testing. The performance metrics were then averaged across all folds to obtain an overall estimate of model accuracy. To provide a clearer view of the model's stability, Table 7 presents the best and worst values of the determination coefficient (R^2) and mean squared error (*MSE*) observed during the five repetitions. The consistent results across all folds confirm the robustness and generalization ability of the proposed framework.

8.2. Phase 2: Assessment under realistic conditions

In practice, the measurement noise should reflect the expected uncertainty of the observed variable in this case, the lattice constant. Literature reports show that DFT calculations of perovskite lattice constants typically deviate from experimental values by 0.5–3 %, depending on the functional, pseudopotential, and structural or temperature effects [84,85]. Yuk et al in [84] reports mean absolute relative errors nearly of 1–2 % for PBE (*Perdew–Burke–Ernzerhof*) functional and LDA (*Local Density Approximation)*, and nearly of 0.8–1 % when using PBEsol

Table 10
Summary of Dataset [6] and Prediction Results for Simple Perovskites Using the Proposed AR-T3FLS-EKF Model.

ABX_3 perovskites	r_A	r_B	r_X	X_A	XB	XX	ZA	ZB	ZX	DA	DB	DX	Actual lattice constant (Å)	Predicted lattice constant (Å)
$AgMgF_3$	1,15	0,72	1,33	1,93	1,31	3,98	47	12	9	10,5	1,74	0,001553	3918	**3917**
$AgNiF_3$	1,15	0,69	1,33	1,93	1,91	3,98	47	28	9	10,5	8,9	0,001553	3936	**3935**
$AgZnF_3$	1,15	0,74	1,33	1,93	1,65	3,98	47	30	9	10,5	7134	0,001553	3972	**3974**
$BaAmO_3$	1,35	0,85	1,4	0,89	1,3	3,44	56	95	8	3,62	12	0,001308	4357	**4361**
$BaCeO_3$	1,35	0,87	1,4	0,89	1,12	3,44	56	58	8	3,62	6,77	0,001308	4397	**4398**
$BaFeO_3$	1,35	0,59	1,4	0,89	1,83	3,44	56	26	8	3,62	7,87	0,001308	3994	**3995**
$BaHfO_3$	1,35	0,71	1,4	0,89	1,3	3,44	56	72	8	3,62	13,3	0,001308	4171	**4173**
$BaMoO_3$	1,35	0,65	1,4	0,89	2,16	3,44	56	42	8	3,62	10,2	0,001308	4,04	**4036**
$BaNbO_3$	1,35	0,68	1,4	0,89	1,6	3,44	56	41	8	3,62	8,57	0,001308	4,08	**4073**
$BaNpO_3$	1,35	0,87	1,4	0,89	1,3	3,44	56	93	8	3,62	20,2	0,001308	4384	**4386**
$BaPaO_3$	1,35	0,9	1,4	0,89	1,5	3,44	56	91	8	3,62	15,4	0,001308	4,45	**4447**
$BaPbO_3$	1,35	0,78	1,4	0,89	1,8	3,44	56	82	8	3,62	11,3	0,001308	4265	**4265**
$BaThO_3$	1,35	0,94	1,4	0,89	1,3	3,44	56	90	8	3,62	11,7	0,001308	4,48	**4481**
$BaUO_3$	1,35	0,89	1,4	0,89	1,7	3,44	56	92	8	3,62	19,1	0,001308	4387	**4388**
$BaZrO_3$	1,35	0,72	1,4	0,89	1,33	3,44	56	40	8	3,62	6,52	0,001308	4193	**4194**
$CaTiO_3$	1	0,61	1,4	1	1,54	3,44	20	22	8	1,54	4506	0,001308	3,84	**3840**
$CeAlO_3$	1,01	0,54	1,4	1,12	1,61	3,44	58	13	8	6,77	2,7	0,001308	3772	**3772**
$CsCaCl_3$	1,67	1	1,81	0,79	1	3,16	55	20	17	1,87	1,54	0,002898	5396	**5398**
$CsCaF_3$	1,67	1	1,33	0,79	1	3,98	55	20	9	1,87	1,54	0,001553	4523	**4531**
$CsCdF_3$	1,67	0,95	1,33	0,79	1,69	3,98	55	48	9	1,87	8,69	0,001553	4,47	**4472**
$CsEuCl_3$	1,67	1,17	1,81	0,79	1,2	3,16	55	63	17	1,87	5,24	0,002898	5627	**5623**
$CsEuF_3$	1,67	1,17	1,33	0,79	1,2	3,98	55	63	9	1,87	5,24	0,001553	4,78	**4782**
$CsHgBr_3$	1,67	1,02	1,96	0,79	1,9	2,96	55	80	35	1,87	13,5336	31,028	5,77	**5769**
$CsHgCl_3$	1,67	1,02	1,81	0,79	1,9	3,16	55	80	17	1,87	13,5336	0,002898	5,41	**5412**
$CsHgF_3$	1,67	1,02	1,33	0,79	1,9	3,98	55	80	9	1,87	13,5336	0,001553	4,57	**4568**
$CsIO_3$	1,67	0,95	1,4	0,79	2,66	3,44	55	53	8	1,87	4933	0,001308	4674	**4676**
$CsPbBr_3$	1,67	1,19	1,96	0,79	1,8	2,96	55	82	35	1,87	11,3	31,028	5874	**5876**
$CsPbCl_3$	1,67	1,19	1,81	0,79	1,8	3,16	55	82	17	1,87	11,3	0,002898	5605	**5609**
$CsPbF_3$	1,67	1,19	1,33	0,79	1,8	3,98	55	82	9	1,87	11,3	0,001553	4,8	**4799**
$CsSnI_3$	1,67	1,02	2,2	0,79	1,96	2,66	55	50	53	1,87	7287	4933	6219	**6221**
$CsSrF_3$	1,67	1,18	1,33	0,79	0,95	3,98	55	38	9	1,87	2,64	0,001553	4,75	**4749**
$CsYbCl_3$	1,67	1,02	1,81	0,79	1,1	3,16	55	70	17	1,87	6,9	0,002898	5437	**5438**
$CsYbF_3$	1,67	1,02	1,33	0,79	1,1	3,98	55	70	9	1,87	6,9	0,001553	4,61	**4611**
$EuCrO_3$	0,95	0,62	1,4	1,2	1,66	3,44	63	24	8	5,24	7,15	0,001308	3803	**3804**
$EuFeO_3$	0,95	0,645	1,4	1,2	1,83	3,44	63	26	8	5,24	7,87	0,001308	3836	**3834**
$EuTiO_3$	0,95	0,67	1,4	1,2	1,54	3,44	63	22	8	5,24	4506	0,001308	3905	**3907**
$GdAlO_3$	0,94	0,54	1,4	1,2	1,61	3,44	64	13	8	7,9	2,7	0,001308	3,71	**3712**

ABX_3 perovskites	r_A	r_B	r_X	X_A	XB	XX	ZA	ZB	ZX	DA	DB	DX	Actual lattice constant (Å)	Predicted lattice constant (Å)
$GdFeO_3$	0,94	0,645	1,4	1,2	1,83	3,44	64	26	8	7,9	7,87	0,001308	3,82	**3826**
$KCdF_3$	1,38	0,95	1,33	0,82	1,69	3,98	19	48	9	0,89	8,69	0,001553	4293	**4296**
$KCoF_3$	1,38	0,74	1,33	0,82	1,88	3,98	19	27	9	0,89	8,86	0,001553	4071	**4065**
$KFeF_3$	1,38	0,78	1,33	0,82	1,83	3,98	19	26	9	0,89	7,87	0,001553	4121	**4116**
$KMgF_3$	1,38	0,72	1,33	0,82	1,31	3,98	19	12	9	0,89	1,74	0,001553	3989	**3991**
$KMnF_3$	1,38	0,83	1,33	0,82	1,55	3,98	19	25	9	0,89	7,3	0,001553	4189	**4184**
$KNbO_3$	1,38	0,64	1,4	0,82	1,6	3,44	19	41	8	0,89	8,57	0,001308	4007	**4007**
$KPaO_3$	1,38	0,78	1,4	0,82	1,5	3,44	19	91	8	0,89	15,4	0,001308	4341	**4339**
$KTaO_3$	1,38	0,64	1,4	0,82	1,5	3,44	19	73	8	0,89	16,4	0,001308	3988	**3990**
KUO_3	1,38	0,76	1,4	0,82	1,7	3,44	19	92	8	0,89	19,1	0,001308	4,29	**4286**
KVF_3	1,38	0,79	1,33	0,82	1,63	3,98	19	23	9	0,89	6	0,001553	4,1	**4101**
$KZnF_3$	1,38	0,74	1,33	0,82	1,65	3,98	19	30	9	0,89	7134	0,001553	4056	**4055**
$LaAlO_3$	1,03	0,54	1,4	1,1	1,61	3,44	57	13	8	6,15	2,7	0,001308	3778	**3780**
$LaCrO_3$	1,03	0,62	1,4	1,1	1,66	3,44	57	24	8	6,15	7,15	0,001308	3874	**3875**
$LaFeO_3$	1,03	0,645	1,4	1,1	1,83	3,44	57	26	8	6,15	7,87	0,001308	3,92	**3922**
$LaCrO_3$	1,03	0,62	1,4	1,1	1,81	3,44	57	31	8	6,15	5,91	0,001308	3874	**3874**
$LaRhO_3$	1,03	0,67	1,4	1,1	2,28	3,44	57	45	8	6,15	12,4	0,001308	3,94	**3936**
$LaFeO_3$	1,03	0,67	1,4	1,1	1,54	3,44	57	22	8	6,15	4506	0,001308	3,92	**3916**
$LiBaF_3$	1,35	0,68	1,33	0,98	0,89	3,98	3	56	9	0,53	3,62	0,001553	3992	**3994**
$NaTaO_3$	1,02	0,64	1,4	0,93	1,5	3,44	11	73	8	0,97	16,4	0,001308	3881	**3877**
$LaRhO_3$	1,02	0,79	1,33	0,93	1,63	3,98	11	23	9	0,97	6	0,001553	3,94	**3934**
$NaWO_3$	1,02	0,62	1,4	0,93	1,7	3,44	11	74	8	0,97	19,3	0,001308	3,85	**3846**
$NdAlO_3$	0,98	0,54	1,4	1,14	1,61	3,44	60	13	8	7,01	2,7	0,001308	3752	**3751**
$NdCoO_3$	0,98	0,55	1,4	1,14	1,88	3,44	60	27	8	7,01	8,86	0,001308	3777	**3779**
$NdCrO_3$	0,98	0,62	1,4	1,14	1,66	3,44	60	24	8	7,01	7,15	0,001308	3835	**3833**
$NdFeO_3$	0,98	0,645	1,4	1,14	1,83	3,44	60	26	8	7,01	7,87	0,001308	3,87	**3868**
$PrCrO_3$	0,99	0,62	1,4	1,13	1,66	3,44	59	24	8	6,77	7,15	0,001308	3852	**3852**
$PrFeO_3$	0,99	0,645	1,4	1,13	1,83	3,44	59	26	8	6,77	7,87	0,001308	3887	**3890**
$PrGaO_3$	0,99	0,62	1,4	1,13	1,81	3,44	59	31	8	6,77	5,91	0,001308	3863	**3860**

(*continued on next page*)

Table 10 (*continued*)

ABX_3 perovskites	r_A	r_B	r_X	X_A	XB	XX	ZA	ZB	ZX	DA	DB	DX	Actual lattice constant (Å)	Predicted lattice constant (Å)
$PrMnO_3$	0,99	0,645	1,4	1,13	1,55	3,44	59	25	8	6,77	7,3	0,001308	3,82	**3821**
$PrVO_3$	0,99	0,64	1,4	1,13	1,63	3,44	59	23	8	6,77	6	0,001308	3,89	**3890**
$RbCaF_3$	1,52	1	1,33	0,82	1	3,98	37	20	9	1,53	1,54	0,001553	4452	**4449**
$RbCdF_3$	1,52	0,95	1,33	0,82	1,69	3,98	37	48	9	1,53	8,69	0,001553	4398	**4395**
$RbMnF_3$	1,52	0,83	1,33	0,82	1,55	3,98	37	25	9	1,53	7,3	0,001553	4,24	**4236**
$RbPaO_3$	1,52	0,78	1,4	0,82	1,5	3,44	37	91	8	1,53	15,4	0,001308	4368	**4361**
$RbPbF_3$	1,52	1,19	1,33	0,82	1,8	3,98	37	82	9	1,53	11,3	0,001553	4,79	**4785**
$RbPdF_3$	1,52	0,86	1,33	0,82	2,2	3,98	37	46	9	1,53	12	0,001553	4298	**4295**
ABX_3 perovskites	r_A	r_B	r_X	X_A	XB	XX	ZA	ZB	ZX	DA	DB	DX	Actual lattice constant (Å)	Predicted lattice constant (Å)
$RbUO_3$	1,52	0,76	1,4	0,82	1,7	3,44	37	92	8	1,53	19,1	0,001308	4323	**4325**
$RbYbF_3$	1,52	1,02	1,33	0,82	1,1	3,98	37	70	9	1,53	6,9	0,001553	4,53	**4532**
$SmAlO_3$	0,96	0,54	1,4	1,17	1,61	3,44	62	13	8	7,52	2,7	0,001308	3734	**3736**
$SmCoO_3$	0,96	0,55	1,4	1,17	1,88	3,44	62	27	8	7,52	8,86	0,001308	3,75	**3754**
$PrVO_3$	0,96	0,64	1,4	1,17	1,63	3,44	62	23	8	7,52	6	0,001308	3,89	**3888**
$SrCoO_3$	1,18	0,53	1,4	0,95	1,88	3,44	38	27	8	2,64	8,86	0,001308	3,85	**3853**
$SrHfO_3$	1,18	0,71	1,4	0,95	1,3	3,44	38	72	8	2,64	13,3	0,001308	4069	**4068**
$SrMoO_3$	1,18	0,65	1,4	0,95	2,16	3,44	38	42	8	2,64	10,2	0,001308	3975	**3972**
$SrNbO_3$	1,18	0,68	1,4	0,95	1,6	3,44	38	41	8	2,64	8,57	0,001308	4016	**4014**
$SrPuO_3$	1,18	0,86	1,4	0,95	1,3	3,44	38	94	8	2,64	19,7	0,001308	4,28	**4282**
$SrSnO_3$	1,18	0,69	1,4	0,95	1,96	3,44	38	50	8	2,64	7287	0,001308	4034	**4038**
$SrTbO_3$	1,18	0,76	1,4	0,95	1,2	3,44	38	65	8	2,64	8,23	0,001308	4,18	**4181**
$SrTcO_3$	1,18	0,65	1,4	0,95	2,1	3,44	38	43	8	2,64	11	0,001308	3949	**3948**
$SrTiO_3$	1,18	0,61	1,4	0,95	1,54	3,44	38	22	8	2,64	4506	0,001308	3905	**3902**
$SrZrO_3$	1,18	0,72	1,4	0,95	1,33	3,44	38	40	8	2,64	6,52	0,001308	4101	**4103**
$TlCdF_3$	1,5	0,95	1,33	1,8	1,69	3,98	81	48	9	11,8	8,69	0,001553	4,4	**4396**
$TlCoF_3$	1,5	0,74	1,33	1,8	1,88	3,98	81	27	9	11,8	8,86	0,001553	4138	**4138**
$TlFeF_3$	1,5	0,78	1,33	1,8	1,83	3,98	81	26	9	11,8	7,87	0,001553	4188	**4190**
$TlMnCl_3$	1,5	0,83	1,81	1,8	1,55	3,16	81	25	17	11,8	7,3	0,002898	5,02	**5018**
$TlMnF_3$	1,5	0,83	1,33	1,8	1,55	3,98	81	25	9	11,8	7,3	0,001553	4,26	**4259**
$TlPdF_3$	1,5	0,86	1,33	1,8	2,2	3,98	81	46	9	11,8	12	0,001553	4301	**4297**
$YAlO_3$	0,9	0,54	1,4	1,22	1,61	3,44	39	13	8	4,47	2,7	0,001308	3,68	**3678**
$YCrO_3$	0,9	0,62	1,4	1,22	1,66	3,44	39	24	8	4,47	7,15	0,001308	3768	**3772**
$YFeO_3$	0,9	0,645	1,4	1,22	1,83	3,44	39	26	8	4,47	7,87	0,001308	3785	**3783**
$AgCoF_3$	1,15	0,74	1,33	1,93	1,88	3,98	47	27	9	10,5	8,86	0,0016	3983	**3993**
$AgMgF_3$	1,15	0,83	1,33	1,93	1,55	3,98	47	25	9	10,5	7,3	0,0016	4,02	**4027**
$AgMnF_3$	1,35	0,63	1,4	0,89	2,2	3,44	56	77	8	3,62	22,56	0,0013	4,1	**4095**
$AgNiF_3$	1,35	0,85	1,4	0,89	1,13	3,44	56	59	8	3,62	6,77	0,0013	4354	**4358**
$AgZnF_3$	1,35	0,69	1,4	0,89	1,96	3,44	56	50	8	3,62	7287	0,0013	4116	**4111**
$BaAmO_3$	1,35	0,67	1,4	0,89	1,54	3,44	56	50	35	1873	4506	31,028	4012	**4025**
$BaCeO_3$	1,67	1,02	1,96	0,79	1,96	2,96	55	50	8	1873	7287	0,0029	5795	**5780**
$BaFeO_3$	1,67	1,01	1,81	0,79	1,25	3,16	55	69	17	9,54	9,32	0,0029	5476	**5457**
$BaHfO_3$	0,95	0,54	1,4	1,2	1,66	3,44	63	13	8	5,24	2,7	0,0013	3725	**3727**
$BaIrO_3$	0,94	0,62	1,4	1,2	1,66	3,44	64	24	8	7,9	7,15	0,0013	3795	**3793**
$BaMoO_3$	1,38	0,69	1,33	0,82	1,91	3,48	19	28	9	0,89	8,9	0,0016	4013	**4014**
$BaNbO_3$	1,03	0,64	1,4	1,1	1,63	3,44	57	23	9	8,15	6	0,0013	3,91	**3914**
$BaNpO_3$	0,99	0,54	1,4	1,13	1,66	3,44	59	13	8	6,77	2,7	0,0013	3757	**3759**
ABX_3 perovskites	r_A	r_B	r_X	X_A	XB	XX	ZA	ZB	ZX	DA	DB	DX	Actual lattice constant (Å)	Predicted lattice constant (Å)
$BaPaO_3$	1,52	0,74	1,33	0,82	1,88	3,98	37	27	9	1,53	8,86	0,0016	4141	**4,143**
$BaPbO_3$	1,52	0,78	1,33	0,82	1,83	3,98	37	26	9	1,53	7,87	0,0016	4174	**4,173**
$BaPrO_3$	1,52	1,02	1,2	1,33	0,95	3,98	37	30	9	1,53	13,53	0,0016	4,47	**4464**
$BaSnO_3$	1,52	0,79	1,33	0,82	1,63	3,98	37	26	9	1,53	6	0,0016	4,17	**4174**
$BaThO_3$	1,52	0,74	1,33	0,82	1,65	3,98	37	30	9	1,53	7134	0,0016	4122	**4117**
$BaTiO_3$	0,96	0,645	1,4	1,33	1,83	3,44	62	26	8	7,52	7,87	0,0013	3845	**3844**
$BaUO_3$	1,02	0,68	1,4	0,89	1,5	3,44	50	73	8	7287	16,4	0,0013	3,88	**3892**
$BaZrO_3$	1,18	0,85	1,4	0,95	1,3	3,44	38	95	8	2,64	12	0,0013	4,23	**4226**
$CaTiO_3$	1,18	0,59	1,4	0,95	1,53	3,44	38	26	8	2,64	7,87	0,0013	3,85	**3849**
$CeAlO_3$	1,18	0,53	1,4	0,95	1,53	3,44	38	25	8	2,64	7,87	0,0013	3,86	**3864**
$CsCaCl_3$	1,18	0,61	1,4	0,95	1,63	3,44	38	23	8	2,64	6	0,0013	3,89	**3886**

(*Perdew–Burke–Ernzerhof solid*) or vdW (*van der Waals*) corrected functionals. You et al in [85] investigate an MD/DFT comparison studies of $CsPbBr_3$ halide perovskites and report deviations of less than 3 % from experimental data. These findings suggest that in realistic scenarios, the measurement noise standard deviation for lattice constants can be reasonably assumed in the range of 0.01–0.05 Å (for lattice constants of ~3–6 Å), corresponding to variances on the order of (10^{-4}–10^{-3}) $Å^2$.

Based on these studies, Gaussian noise with two standard deviation levels (0.01 and 0.05 Å) was added to the datasets [5,6]. For each noise level, two measurement noise covariance values were considered (R = 0.001 and $\boldsymbol{R}$ = 0.0001), while the process noise covariance $\boldsymbol{Q}$ was varied in each case. The $\boldsymbol{Q}$ matrix represents the covariance of the process noise and quantifies uncertainty in the system dynamics. Larger values of $\boldsymbol{Q}$ indicate less confidence in the model, leading the EKF to rely more on measurements. Conversely, smaller $\boldsymbol{Q}$ values imply greater trust in the model. The $\boldsymbol{R}$ matrix represents the covariance of the measurement noise and quantifies uncertainty in the observations. Larger $\boldsymbol{R}$ values make the EKF rely more on model predictions, while smaller $\boldsymbol{R}$

Table 11
Summary of Dataset [5] and Prediction Results for Simple Perovskites Using the Proposed AR-T3FLS-EKF Model.

ABX_3 perovskites	r_A	r_B	r_X	t	Actual lattice constant (Å)	Predicted lattice constant (Å)
$CsIO_3$	1,67	0,95	1,4	0,829	4674	**4672**
$RbUO_3$	1,52	0,76	1,4	0,906	4323	**4325**
KUO_3	1,38	0,76	1,4	0,919	4,29	**4289**
$RbPaO_3$	1,52	0,78	1,4	0,898	4368	**4368**
$KPaO_3$	1,38	0,78	1,4	0,91	4341	**4340**
$KTaO_3$	1,38	0,64	1,4	0,973	3988	**3993**
$KNiF_3$[a]	1,38	0,69	1,33	0,926	4013	**4012**
$BaNbO_3$	1,35	0,68	1,4	0,958	4,08	**4081**
$BaHfO_3$	1,35	0,71	1,4	0,944	4171	**4174**
$BaZrO_3$	1,35	0,72	1,4	0,939	4193	**4191**
$BaIrO_3$	1,35	0,63	1,4	0,982	4,1	**4097**
$EuTiO_3$	0,95	0,67	1,4	1026	3905	**3906**
$NaWO_3$	1,02	0,62	1,4	1043	3,85	**3847**
$SnTaO_3$	1,02	0,68	1,4	1007	3,88	**3879**
$SrMnO_3$	1,18	0,53	1,4	1067	3806	**3807**
$SrNbO_3$[b]	1,18	0,68	1,4	0,981	4016	**4014**
$SrVO_3$	1,18	0,61	1,4	1019	3,89	**3889**
$SrMoO_3$	1,18	0,65	1,4	0,997	3975	**3974**
$SrSnO_3$	1,18	0,69	1,4	0,976	4034	**4033**
$SrAmO_3$[a]	1,18	0,85	1,4	0,899	4,23	**4228**
$SrHfO_3$	1,18	0,71	1,4	0,965	4069	**4072**
$BaPbO_3$	1,35	0,78	1,4	0,913	4265	**4267**
$BaMoO_3$[b]	1,35	0,65	1,4	0,972	4,04	**4041**
$BaPrO_3$	1,35	0,85	1,4	0,884	4354	**4355**
$BaCeO_3$	1,35	0,87	1,4	0,876	4397	**4397**
$BaAmO_3$	1,35	0,85	1,4	0,884	4357	**4358**
$BaNpO_3$[a]	1,35	0,87	1,4	0,876	4384	**4386**
$BaUO_3$	1,35	0,89	1,4	0,868	4387	**4390**
$BaPaO_3$	1,35	0,9	1,4	0,864	4,45	**4446**
$BaSnO_3$[b]	1,35	0,69	1,4	0,953	4116	**4113**
$BaThO_3$	1,35	0,94	1,4	0,849	4,48	**4478**
$SrTbO_3$	1,18	0,76	1,4	0,94	4,18	**4182**
$SrTiO_3$[b]	1,18	0,61	1,4	1019	3905	**3906**
$SrPuO_3$	1,18	0,86	1,4	0,894	4,28	**4280**
$SrCoO_3$[a]	1,18	0,53	1,4	1067	3,85	**3850**
$BaTiO_3$	1,35	0,61	1,4	0,992	4012	**4012**
ABX_3 perovskites	r_A	r_B	r_X	t	Actual lattice constant (Å)	Predicted lattice constant (Å)
$CaTiO_3$	1	0,61	1,4	1054	3,84	**3840**
$CeAlO_3$	1,01	0,54	1,4	1099	3772	**3773**
$EuAlO_3$	0,95	0,54	1,4	1115	3725	**3725**
$EuCrO_3$	0,95	0,62	1,4	1058	3803	**3803**
$EuFeO_3$	0,95	0,645	1,4	1042	3836	**3829**
$GdAlO_3$	0,94	0,54	1,4	1118	3,71	**3710**
$GdFeO_3$	0,94	0,645	1,4	1044	3,82	**3818**
$GdCrO_3$[a]	0,94	0,62	1,4	1061	3795	**3797**
$KNbO_3$	1,38	0,64	1,4	0,973	4007	**4008**
$LaAlO_3$	1,03	0,54	1,4	1094	3778	**3780**
$LaCrO_3$	1,03	0,62	1,4	1041	3874	**3877**
$LaFeO_3$	1,03	0,645	1,4	1026	3,92	**3924**
$LaRhO_3$	1,03	0,67	1,4	1011	3,94	**3938**
$LaTiO_3$	1,03	0,67	1,4	1011	3,92	**3915**
$LaVO_3$	1,03	0,64	1,4	1029	3,91	**3913**
$NaTaO_3$	1,02	0,64	1,4	1031	3881	**3878**
$NdFeO_3$[a]	0,98	0,645	1,4	1036	3,87	**3868**
$NdCoO_3$	0,98	0,55	1,4	1,1	3777	**3775**
$NdAlO_3$[b]	0,98	0,54	1,4	1107	3752	**3753**
$NdCrO_3$[b]	0,98	0,62	1,4	1052	3835	**3834**
$PrAlO_3$	0,99	0,54	1,4	1105	3757	**3760**
$PrCrO_3$	0,99	0,62	1,4	1,05	3852	**3853**
$PrFeO_3$	0,99	0,645	1,4	1034	3887	**3891**
$PrGaO_3$	0,99	0,62	1,4	1,05	3863	**3865**
$PrMnO_3$	0,99	0,645	1,4	1034	3,82	**3822**
$PrVO_3$	0,99	0,64	1,4	1037	3,89	**3892**
$LaGaO_3$[a]	1,03	0,62	1,4	1041	3874	**3874**

(*continued on next page*)

Table 11 (*continued*)

ABX_3 perovskites	r_A	r_B	r_X	t	Actual lattice constant (Å)	Predicted lattice constant (Å)
$SmCoO_3$	0,96	0,55	1,4	1105	3,75	**3752**
$SmVO_3$[a]	0,96	0,64	1,4	1043	3,89	**3892**
$SmAlO_3$[a]	0,96	0,54	1,4	1113	3734	**3737**
$SmFeO_3$	0,96	0,645	1,4	1,04	3845	**3840**
$SrZrO_3$	1,18	0,72	1,4	0,96	4101	**4105**
$YAlO_3$	0,9	0,54	1,4	1129	3,68	**3681**
$YFeO3$[b]	0,9	0,645	1,4	1053	3785	**3787**
$YCrO_3$	0,9	0,62	1,4	1,07	3768	**3766**
$CsCdF_3$	1,67	0,95	1,33	0,81	4,47	**4474**
ABX_3 perovskites	r_A	r_B	r_X	t	Actual lattice constant (Å)	Predicted lattice constant (Å)
$CsCaF_3$	1,67	1	1,33	0,795	4523	**4527**
$CsHgF_3$	1,67	1,02	1,33	0,789	4,57	**4569**
$CsSrF_3$	1,67	1,18	1,33	0,744	4,75	**4749**
$TlCoF3$	1,5	0,74	1,33	0,893	4138	**4136**
$BaFeO_3$[a]	1,35	0,59	1,4	1002	3994	**3997**
$SrFeO_3$[a]	1,18	0,59	1,4	1031	3,85	**3849**
$TlFeF_3$	1,5	0,78	1,33	0,878	4188	**4187**
$TlMnF3$	1,5	0,83	1,33	0,859	4,26	**4260**
$NH4ZnF_3$	1,48	0,74	1,33	0,895	4115	**4113**
$NH4CoF_3$	1,48	0,74	1,33	0,895	4129	**4129**
$NH4FeF_3$	1,48	0,78	1,33	0,879	4177	**4175**
$NH4MnF_3$	1,48	0,83	1,33	0,86	4241	**4239**
$RbZnF_3$	1,52	0,74	1,33	0,892	4122	**4121**
$RbCoF_3$	1,52	0,74	1,33	0,892	4141	**4139**
$RbFeF_3$	1,52	0,78	1,33	0,876	4174	**4175**
$RbMnF_3$	1,52	0,83	1,33	0,858	4,24	**4239**
$RbCdF_3$	1,52	0,95	1,33	0,816	4398	**4396**
$RbCaF_3$	1,52	1	1,33	0,8	4452	**4449**
$RbHgF_3$	1,52	1,02	1,33	0,793	4,47	**4467**
$KCdF_3$	1,38	0,95	1,33	0,822	4293	**4299**
$KMgF_3$	1,38	0,72	1,33	0,913	3989	**3994**
$KZnF_3$	1,38	0,74	1,33	0,904	4056	**4053**
$KCoF_3$	1,38	0,74	1,33	0,904	4071	**4069**
KVF_3[b]	1,38	0,79	1,33	0,883	4,1	**4099**
$KFeF_3$	1,38	0,78	1,33	0,887	4121	**4122**
$KMnF_3$	1,38	0,83	1,33	0,867	4189	**4187**
$AgMgF_3$	1,15	0,72	1,33	0,938	3918	**3914**
$AgCoF_3$[b]	1,15	0,74	1,33	0,928	3983	**3982**
$AgNiF_3$	1,15	0,69	1,33	0,953	3936	**3931**
$AgZnF_3$	1,15	0,74	1,33	0,928	3972	**3978**
$AgMnF_3$	1,15	0,83	1,33	0,886	4,03	**4028**
$NaVF_3$	1,02	0,79	1,33	0,918	3,94	**3939**
$RbPdF_3$	1,52	0,86	1,33	0,847	4298	**4296**
$RbVF_3$[b]	1,52	0,79	1,33	0,872	4,17	**4181**
$NH4MgF_3$	1,48	0,72	1,33	0,903	4,06	**4061**
$TlPdF_3$	1,5	0,86	1,33	0,848	4301	**4300**
ABX_3 perovskites	r_A	r_B	r_X	t	Actual lattice constant (Å)	Predicted lattice constant (Å)
$LiBaF_3$	1,35	0,68	1,33	0,934	3992	**3994**
$RbYbF_3$	1,52	1,02	1,33	0,793	4,53	**4531**
$CsEuF_3$	1,67	1,17	1,33	0,747	4,78	**4782**
$CsPbF_3$	1,67	1,19	1,33	0,742	4,8	**4803**
$CsYbF_3$	1,67	1,02	1,33	0,789	4,61	**4611**
$RbPbF_3$	1,52	1,19	1,33	0,744	4,79	**4777**
$CsCaCl_3$	1,67	1	1,81	0,922	5396	**5394**
$CsPbCl_3$	1,67	1,19	1,81	0,86	5605	**5608**
$CsHgCl_3$	1,67	1,02	1,81	0,915	5,41	**5413**
$TlMnCl_3$	1,5	0,83	1,81	1005	5,02	**5019**
$TlCdF3$[b]	1,5	0,95	1,33	0,817	4,4	**4398**
$CsEuCl_3$	1,67	1,17	1,81	0,866	5627	**5625**
$CsTmCl_3$	1,67	1,01	1,81	0,918	5476	**5476**
$CsYbCl_3$[b]	1,67	1,02	1,81	0,915	5437	**5438**
$CsHgBr_3$	1,67	1,02	1,96	0,954	5,77	**5765**
$CsPbBr_3$	1,67	1,19	1,96	0,897	5874	**5876**
$CsSnBr_3$	1,67	1,02	1,96	0,954	5795	**5788**

(*continued on next page*)

Table 11 (*continued*)

ABX_3 perovskites	r_A	r_B	r_X	t	Actual lattice constant (Å)	Predicted lattice constant (Å)
$CsSnI_3$	1,67	1,02	2,2	1017	6219	**6202**
$SrTcO_3$ [a]	1,18	0,65	1,4	0,997	3949	**3943**

values increase trust in the measurements. Finally, a sensitivity analysis of the results was performed using several criteria, including the Mean Squared Error (*MSE*), Root Mean Squared Error (*RMSE*), and Mean Absolute Error (*MAE*).

The numerical results of the sensitivity analysis of the Extended Kalman Filter under realistic conditions are summarized in Tables 8 and 9.

The sensitivity analysis (Table 8 and Table 9) demonstrates that the extended kalman filter performance is highly dependent on the proper selection of the process noise covariance $\boldsymbol{Q}$ and the measurement noise covariance $\boldsymbol{R}$. The optimal configuration, obtained at $\boldsymbol{Q}$ = 1.00E−06 and $\boldsymbol{R}$ = 0.001, indicates a balanced trade-off between model dynamics and measurement reliability. When $\boldsymbol{Q}$ was too small ($\boldsymbol{Q}$ = 1.00E−9), the filter relied excessively on the internal model, leading to slower adaptation to variations induced by the added Gaussian noise. This caused an accumulation of estimation errors, particularly under higher noise levels. Conversely, when $\boldsymbol{Q}$ was too large ($\boldsymbol{Q}$ = 1.00E−3) the EKF became overly sensitive to measurement fluctuations, resulting in unstable or noisy estimates. Similarly, the effect of $\boldsymbol{R}$ reflects the role of measurement trust. A smaller $\boldsymbol{R}$ ($\boldsymbol{R}$ = 0.0001) led to excessive reliance on noisy observations, slightly degrading performance, while a larger $\boldsymbol{R}$ ($\boldsymbol{R}$ = 0.001) provided more stable filtering and smoother convergence. Overall, the results confirm that a moderate level of process noise ($\boldsymbol{Q}$ = 1.00E−6) and a higher measurement noise covariance ($\boldsymbol{R}$ = 0.001) yield the best compromise, enabling the filter to adapt effectively to system uncertainty without overreacting to measurement noise. This configuration maintains prediction stability and minimizes the error metrics (*MSE, RMSE, MAE*) across both Gaussian noise levels.

The superiority of the proposed AR–T3FLS–EKF framework extends beyond predictive accuracy and stems from its intrinsic design. The autoregressive component enables recursive modeling of compositional dependencies, allowing the system to capture structured feature interactions. The Interval Type-3 fuzzy logic enhances uncertainty handling through the footprint of uncertainty, while the Extended Kalman Filter introduces gradient-aware parameter tuning and robust adaptation to measurement and process noise. Unlike benchmark models such as SVR and GPR, which suffer from kernel rigidity and operate as black-box predictors, the proposed approach combines transparency, adaptability, and noise robustness through its fuzzy rule structure and dynamic state estimation. This synergy explains its superior generalization capability and stronger physical consistency:

1. Autoregressive reasoning, which enables recursive modeling of interdependent compositional descriptors, allowing the system to capture structured feature dependencies ignored by static models;
2. Interval Type-3 fuzzy logic, which provides explicit modeling of higher-order and epistemic uncertainty through the footprint of uncertainty, improving generalization under scarce or noisy data;
3. Extended Kalman filtering, which introduces gradient-aware parameter tuning and adaptive state estimation, enhancing convergence stability and robustness to noise.

Finally, all the datasets used in this study are comprehensively presented in Tables 10–12 with the accurate prediction results achieved by the proposed model.

Table 12
Summary of Dataset [7] and Prediction Results for Double Perovskites Using the Proposed AR-T3FLS Model.

$A_2BB'X_6$ perovskites	r_A	r_B	$r_{B'}$	x_B	$x_{B'}$	z_B	Actual lattice constant (Å)	Predicted lattice constant (Å)
Ba_2AgIO_6	1,61	1,15	0,53	1,93	2,66	1	8,46	**8465**
Ba_2LiOsO_6	1,61	0,76	0,53	0,98	2,2	1	8105	**8108**
Ba_2NaIO_6	1,61	1,02	0,53	0,93	2,66	1	8,33	**8320**
Ba_2NaOsO_6	1,61	1,02	0,53	0,93	2,2	1	8287	**8278**
Ca_2LiOsO_6	1,34	0,76	0,53	0,98	2,2	1	7,83	**7833**
Ca_2LiReO_6	1,34	0,76	0,53	0,98	1,9	1	7,83	**7831**
Sr_2LiReO_6	1,44	0,76	0,53	0,98	1,9	1	7,87	**7868**
Sr_2NaOsO_6	1,44	1,02	0,53	0,93	2,2	1	8,13	**8133**
Ba_2BiTaO_6	1,61	1,03	0,64	1,9	1,5	3	8568	**8567**
Ba_2CePaO_6	1,61	1,01	0,78	1,12	1,5	3	8,8	**8798**
Ba_2DyNbO_6	1,61	0,91	0,64	1,22	1,6	3	8437	**8437**
Ba_2DyPaO_6	1,61	0,91	0,78	1,22	1,5	3	8,74	**8742**
Ba_2ErNbO_6	1,61	0,89	0,64	1,24	1,6	3	8427	**8428**
Ba_2ErPaO_6	1,61	0,89	0,78	1,24	1,5	3	8716	**8717**
Ba_2ErRuO_6	1,61	0,89	0,57	1,24	2,2	3	8323	**8325**
Ba_2ErTaO_6	1,61	0,89	0,64	1,24	1,5	3	8423	**8420**
Ba_2EuNbO_6	1,61	0,95	0,64	1,12	1,6	3	8507	**8510**
Ba_2EuPaO_6	1,61	0,95	0,78	1,12	1,5	3	8783	**8784**
Ba_2FeMoO_6	1,61	0,65	0,61	1,83	2,16	3	8075	**8081**
Ba_2FeReO_6	1,61	0,65	0,58	1,83	1,9	3	8,05	**8060**
Ba_2GdPaO_6	1,61	0,94	0,78	1,2	1,5	3	8774	**8769**
Ba_2GdReO_6	1,61	0,94	0,58	1,2	1,9	3	8431	**8436**
Ba_2HoNbO_6	1,61	0,9	0,64	1,23	1,6	3	8434	**8435**
Ba_2HoPaO_6	1,61	0,9	0,78	1,23	1,5	3	8,73	**8731**
Ba_2InNbO_6	1,61	0,8	0,64	1,78	1,6	3	8279	**8275**
Ba_2InOsO_6	1,61	0,8	0,58	1,78	2,2	3	8224	**8223**
Ba_2InReO_6	1,61	0,8	0,58	1,78	1,9	3	8258	**8261**
Ba_2InSbO_6	1,61	0,8	0,6	1,78	2,05	3	8269	**8276**
Ba_2InUO_6	1,61	0,8	0,76	1,78	1,7	3	8,52	**8519**
Ba_2LaPaO_6	1,61	1,03	0,78	1,1	1,5	3	8885	**8889**
Ba_2LuNbO_6	1,61	0,86	0,64	1	1,6	3	8364	**8352**
Ba_2LuPaO_6	1,61	0,86	0,78	1	1,5	3	8666	**8655**
Ba_2MnReO_6	1,61	0,65	0,58	1,55	1,9	3	8,18	**8162**
Ba_2NdNbO_6	1,61	0,98	0,64	1,14	1,6	3	8,54	**8546**
Ba_2NdReO_6	1,61	0,98	0,58	1,14	1,9	3	8,51	**8506**
Ba_2NdTaO_6	1,61	0,98	0,64	1,14	1,5	3	8556	**8556**
Ba_2RhNbO_6	1,61	0,75	0,64	2,28	1,6	3	8,17	**8166**
Ba_2ScNbO_6	1,61	0,75	0,64	1,36	1,6	3	8234	**8235**
Ba_2ScPaO_6	1,61	0,75	0,78	1,36	1,5	3	8549	**8547**
Ba2ScReO$_6$	1,61	0,75	0,58	1,36	1,9	3	8163	**8156**
Ba_2ScTaO_6	1,61	0,75	0,64	1,36	1,5	3	8231	**8232**
Ba_2ScUO_6	1,61	0,75	0,76	1,36	1,7	3	8,49	**8478**
Ba_2SmPaO_6	1,61	0,96	0,78	1,17	1,5	3	8792	**8794**
Ba_2SmTaO_6	1,61	0,96	0,64	1,17	1,5	3	8519	**8521**
Ba_2TlSbO_6	1,61	0,89	0,6	1,8	2,05	3	8381	**8382**
Ba_2TlTaO_6	1,61	0,89	0,64	1,8	1,5	3	8,42	**8420**
Ba_2TmPaO_6	1,61	0,88	0,78	1,25	1,5	3	8692	**8694**
Ba_2TmTaO_6	1,61	0,88	0,64	1,25	1,5	3	8406	**8405**
Ba_2YPaO_6	1,61	0,9	0,78	1,22	1,5	3	8718	**8723**
Ba_2YReO_6	1,61	0,9	0,58	1,22	1,9	3	8372	**8374**
Ba_2YUO_6	1,61	0,9	0,76	1,22	1,7	3	8,69	**8690**
Ba_2YbNbO_6	1,61	0,87	0,64	1,21	1,6	3	8374	**8369**
Ba_2YbTaO_6	1,61	0,87	0,64	1,21	1,5	3	8,39	**8387**
Pb_2ScTaO_6	1,49	0,75	0,64	1,36	1,5	3	8,14	**8142**
Sr_2AlTaO_6	1,44	0,54	0,64	1,61	1,5	3	7791	**7793**
Sr_2CoSbO_6	1,44	0,61	0,6	1,88	2,05	3	7,88	**7886**
Sr_2CrOsO_6	1,44	0,62	0,58	1,66	2,2	3	7,84	**7837**
Sr_2CrWO_6	1,44	0,62	0,62	1,66	1,7	3	7,82	**7816**
Sr_2GaOsO_6	1,44	0,62	0,58	1,81	2,2	3	7,82	**7816**
Sr_2GaReO_6	1,44	0,62	0,58	1,81	1,9	3	7843	**7850**
Sr_2InReO_6	1,44	0,8	0,58	1,78	1,9	3	8071	**8070**

(*continued on next page*)

Table 12 (*continued*)

$A_2BB'X_6$ perovskites	r_A	r_B	$r_{B'}$	x_B	$x_{B'}$	z_B	Actual lattice constant (Å)	Predicted lattice constant (Å)
Sr_2InUO_6	1,44	0,8	0,76	1,78	1,7	3	8,33	**8331**
Sr_2ScBiO_6	1,44	0,75	0,76	1,36	1,9	3	8182	**8182**
Sr_2ScOsO_6	1,44	0,75	0,58	1,36	2,2	3	8,02	**8024**
Sr_2RhTaO_6	1,44	0,67	0,64	2,28	1,5	3	7939	**7937**
Sr_2CrNbO_6	1,44	0,62	0,64	1,66	1,6	3	7,87	**7864**
Ba_2CaMoO_6	1,61	1	0,59	1	2,16	2	8,38	**8377**
Ba_2CaOsO_6	1,61	1	0,55	1	2,2	2	8362	**8362**
Ba_2CaTeO_6	1,61	1	0,56	1	2,1	2	8393	**8398**
Ba_2CaUO_6	1,61	1	0,73	1	1,7	2	8,67	**8665**
Ba_2CdMoO_6	1,61	0,95	0,59	1,69	2,16	2	8324	**8322**
Ba_2CdOsO_6	1,61	0,95	0,55	1,69	2,2	2	8325	**8325**
Ba_2CoMoO_6	1,61	0,75	0,59	1,88	2,16	2	8086	**8081**
Ba_2CoReO_6	1,61	0,75	0,55	1,88	1,9	2	8086	**8084**
Ba_2CoWO_6	1,61	0,75	0,6	1,88	1,7	2	8108	**8101**
Ba_2CrUO_6	1,61	0,8	0,73	1,66	1,7	2	8297	**8307**
Ba_2FeUO_6	1,61	0,78	0,73	1,83	1,7	2	8312	**8319**
Ba_2MgMoO_6	1,61	0,72	0,59	1,31	2,16	2	8084	**8078**
Ba_2MgReO_6	1,61	0,72	0,55	1,31	1,9	2	8082	**8082**
Ba_2MgTeO_6	1,61	0,72	0,56	1,31	2,1	2	8,13	**8131**
Ba_2MgWO_6	1,61	0,72	0,6	1,31	1,7	2	8098	**8100**
Ba_2MnMoO_6	1,61	0,83	0,59	1,55	2,16	2	8168	**8170**
Ba_2MnUO_6	1,61	0,83	0,73	1,55	1,7	2	8,52	**8524**
Ba_2NiMoO_6	1,61	0,69	0,59	1,91	2,16	2	8035	**8035**
Ba_2NiUO_6	1,61	0,69	0,73	1,91	1,7	2	8336	**8336**
Ba_2NiWO_6	1,61	0,69	0,6	1,91	1,7	2	8075	**8072**
Ba_2ZnOsO_6	1,61	0,74	0,55	1,65	2,2	2	8095	**8093**
Ba_2ZnReO_6	1,61	0,74	0,55	1,65	1,9	2	8106	**8113**
Ba_2ZnWO_6	1,61	0,74	0,6	1,65	1,7	2	8116	**8112**
Ca_2CaWO_6	1,34	1	0,6	1	1,7	2	8	**8003**
Pb_2FeWO_6	1,49	0,78	0,6	1,83	1,7	2	8,05	**8043**
Pb_2MgTeO_6	1,49	0,72	0,56	1,31	2,1	2	7,99	**7994**
Sr_2CaOsO_6	1,44	1	0,55	1	2,2	2	8,21	**8209**
Sr_2CoUO_6	1,44	0,75	0,73	1,88	1,7	2	8,19	**8187**
Sr_2FeOsO_6	1,44	0,78	0,55	1,83	2,2	2	7,85	**7871**
Sr_2FeUO_6	1,44	0,78	0,73	1,83	1,7	2	8,11	**8104**
Sr_2MgUO_6	1,44	0,72	0,73	1,31	1,7	2	8,19	**8189**
Sr_2MnUO_6	1,44	0,83	0,73	1,55	1,7	2	8,28	**8283**
Ba_2LiReO_6	1,61	0,76	0,58	0,98	1,9	1	8118	**8120**
Ba_2NaReO_6	1,61	1,02	0,58	0,93	1,9	1	8296	**8304**
Sr_2LiOsO_6	1,44	0,76	0,53	0,98	2,2	1	7,86	**7854**
Sr_2NaReO_6	1,44	1,02	0,58	0,93	1,9	1	8,13	**8134**
Ba_2CoReO_6	1,61	0,75	0,58	1,88	1,9	2	8086	**8083**
Ba_2DyTaO_6	1,61	0,91	0,64	1,22	1,5	3	8545	**8543**
Ba_2ErReO_6	1,61	0,89	0,58	1,24	1,9	3	8354	**8352**
Ba_2ErUO_6	1,61	0,89	0,89	1,24	1,38	3	8,67	**8677**
Ba_2EuTaO_6	1,61	0,95	0,95	1,12	1,5	3	8506	**8498**
Ba_2GdNbO_6	1,61	0,94	0,64	1,2	1,6	3	8496	**8497**
Ba_2GdSbO_6	1,61	0,94	0,6	1,2	2,05	3	8,44	**8433**
$Ba2HoTaO_6$	1,61	0,9	0,95	1,23	1,5	3	8442	**8446**
Ba_2InPaO_6	1,61	0,8	0,78	1,78	1,5	3	8596	**8599**
Ba_2InTaO_6	1,61	0,8	0,95	1,78	1,5	3	8,28	**8278**
Ba_2LaReO_6	1,61	1,03	0,53	1,1	1,9	3	8,58	**8577**
Ba_2LuTaO_6	1,61	0,86	0,95	1	1,5	3	8372	**8385**
Ba_2NdPaO_6	1,61	0,98	0,78	1,14	1,5	3	8,84	**8846**
Ba_2PrPaO_6	1,61	0,99	0,78	1,13	1,5	3	8862	**8852**
Ba_2ScOsO_6	1,61	0,75	0,53	1,36	2,2	3	8152	**8156**
Ba_2ScSbO_6	1,61	0,75	0,6	1,36	2,05	3	8197	**8197**
Ba_2SmNbO_6	1,61	0,96	0,64	1,17	1,6	3	8518	**8519**
Ba_2TbPaO_6	1,61	0,92	0,78	1,1	1,5	3	8753	**8758**
Ba_2TmNbO_6	1,61	0,88	0,64	1,25	1,6	3	8408	**8408**
Ba_2YNbO_6	1,61	0,9	0,64	1,22	1,6	3	8441	**8438**
Ba_2YTaO_6	1,61	0,9	0,64	1,22	1,5	3	8433	**8433**

(*continued on next page*)

Table 12 (*continued*)

$A_2BB'X_6$ perovskites	r_A	r_B	$r_{B'}$	x_B	$x_{B'}$	z_B	Actual lattice constant (Å)	Predicted lattice constant (Å)
Ba_2YbPaO_6	1,61	0,87	0,78	1,21	1,5	3	8678	**8680**
Sr_2AlNbO_6	1,44	0,54	0,64	1,61	1,6	3	7786	**7794**
Sr_2CrMoO_6	1,44	0,62	0,59	1,66	2,16	3	7,84	**7822**
Sr_2FeBiO_6	1,44	0,78	0,76	1,83	1,9	3	8063	**8068**
Sr_2InOsO_6	1,44	0,8	0,58	1,78	2,2	3	8,06	**8062**
Sr_2RhNbO_6	1,44	0,75	0,64	2,28	1,6	3	7914	**7933**
Sr_2ScReO_6	1,44	0,75	0,53	1,36	1,9	3	8,02	**8020**
Ba_2BaUO_6	1,61	1,61	0,76	0,89	1,38	3	8,89	**8896**
Ba_2CaReO_6	1,61	1,34	0,58	1	1,9	2	8356	**8357**
Ba_2CaWO_6	1,61	1,34	0,62	1	2,36	2	8388	**8422**
Ba_2CdReO_6	1,61	0,95	0,58	1,69	1,9	2	8322	**8312**
Ba_2CoUO_6	1,61	0,75	0,76	1,88	1,38	2	8374	**8380**
Ba_2FeReO_6	1,61	0,78	0,58	1,83	1,9	2	8,05	**8081**
Ba_2MgOsO_6	1,61	0,72	0,58	1,31	2,2	2	8,08	**8062**
Ba_2MgUO_6	1,61	0,72	0,76	1,31	1,38	2	8381	**8377**
Ba_2MnWO_6	1,61	0,83	0,62	1,55	2,36	2	8199	**8205**
Ba_2NiReO_6	1,61	0,69	0,58	1,91	1,9	2	8,04	**8035**
Ba_2ZnMoO_6	1,61	0,74	0,59	1,65	2,16	2	8103	**8080**
Ba_2ZnUO_6	1,61	0,74	0,76	1,65	1,38	2	8397	**8398**
Ca_2MgWO_6	1,34	0,72	0,62	1,31	2,36	2	7,7	**7746**
Pb_2MgWO_6	1,49	0,72	0,62	1,31	2,36	2	8006	**8005**
Sr_2CrUO_6	1,44	0,62	0,76	1,66	1,38	2	8,09	**8086**
Sr_2MgTeO_6	1,44	0,72	0,56	1,31	2,1	2	7,94	**7940**
Sr_2NiUO_6	1,44	0,69	0,76	1,91	1,38	2	8,15	**8161**

9. Conclusion

In this study, we proposed and validated an Autoregressive Type-3 Fuzzy Logic System optimized with the Extended Kalman Filter (AR-T3FLS-EKF) to accurately predict lattice constants in both simple and double perovskite materials. The suggested technique combines autoregressive modeling with Type-3 fuzzy logic's better uncertainty management, while the EKF acts as an efficient online tuning mechanism for membership function parameters such as centers, widths, and horizontal slices. This combination guarantees versatility and great prediction accuracy. The process was thoroughly tested in three stages. First, a comparison with a traditional Type-3 fuzzy logic model revealed a significant performance advantage for the suggested AR-T3FLS-EKF, as seen by tighter alignment in output superposition plots and stronger correlation in linear fit curves. Our technique outperformed recently published approaches in terms of predicted accuracy, as measured by *RMSE*, *MAE*, and R^2 in the second step. Finally, a generalization test using previously unreported simple perovskite datasets proved the model's resilience, demonstrating consistent performance and stability across multiple data distributions. Overall, the proposed AR-T3FLS-EKF outperforms traditional fuzzy systems in terms of accuracy while also providing improved flexibility and generalization capabilities, making it a desirable computational tool for materials science applications. Its capacity to capture nonlinear connections and successfully integrate uncertainty implies that it may be used to various material property prediction tasks, hence facilitating rapid materials discovery. The results of this work significantly emphasize the need of hybrid intelligent systems for complicated scientific prediction challenges. The suggested framework may be used as a reference model for future research in computational materials science and engineering. It enables faster and more reliable material property estimation by connecting data-driven knowledge with physical insights. Finally, the proposed AR-T3FLS-EKF framework has certain limitations that open perspectives for future research. The robustness of the model to measurement and process noise is enhanced by the EKF adaptation and the Type-3 fuzzy representation of uncertainty; however, its accuracy may still depend on the initialization of filter parameters and the availability of representative compositional features. Furthermore, the current validation has been conducted on small to medium-sized datasets, and future work will explore scala-

bility to larger and more diverse materials databases through incremental or distributed learning strategies. Beyond lattice constant prediction, the proposed approach can be extended to a broad range of scientific and engineering problems where uncertainty modeling and limited data remain critical challenges, such as thermal stability analysis, phase transition prediction, and multi-sensor data fusion.

CRediT authorship contribution statement

Mohammed Assam Ouali: Writing – review & editing, Writing – original draft, Visualization, Validation, Supervision, Software, Resources, Project administration, Methodology, Investigation, Funding acquisition, Formal analysis, Data curation, Conceptualization. **Hamza Bennacer:** Writing – review & editing, Writing – original draft, Validation, Supervision, Resources, Project administration, Methodology, Investigation, Funding acquisition, Formal analysis, Data curation, Conceptualization. **Mohamed Ladjal:** Writing – review & editing. **Inas Bouzateur:** Writing – review & editing.

Declaration of competing interest

The authors declare that they have no known competing financial interests or personal relationships that could have appeared to influence the work reported in this paper.

Data availability

This article includes all data produced or analyzed during this study. Extra data will be made available on request.

References

[1] Wei Wang, et al., Research progress of perovskite materials in Photocatalysis- and photovoltaics-related energy conversion and environmental treatment, Chem. Soc. Rev. 44 (2015) 5371–5408, https://doi.org/10.1039/C5CS00113G.

[2] Mohsin Afroz, et al., Perovskite solar cells: Progress, challenges, and future avenues to clean energy, Sol. Energy 287 (2025) 113205, https://doi.org/10.1016/j.solener.2024.113205.

[3] Ahmad Ayyaz, Et al. "optoelectronic and transport response of double perovskites Na2AuMX6 (M= Al, Ga, and X= Br, I) for energy harvesting: a DFT investigation.", Mater. Sci. Eng. B 316 (2025) 118133, https://doi.org/10.1016/j.mseb.2025.118133.

[4] Mary Anne White, Physical Properties of Materials, Third Edition, October 2018, CRC Press, ISBN-10: 1138569178.

[5] I. Bouzateur, et al., Perovskite lattice constant prediction framework using optimized artificial neural network and fuzzy logic models by metaheuristic algorithms, Mater. Today Commun. 37 (2023) 107021, https://doi.org/10.1016/j.mtcomm.2023.107021.

[6] Abdulgafor Alfares, Yusuf Abubakar Sha'aban, Ahmed Alhumoud, Machine learning-driven predictions of lattice constants in ABX_3 perovskite materials, Eng. Appl. Artif. Intell. 141 (2025) 109747, https://doi.org/10.1016/j.engappai.2024.109747.

[7] Yun Zhang, Xu Xiaojie, Machine learning lattice constants for cubic perovskite A_2^{2+} $BB'O_6$ compounds, CrystEngComm 22 (38) (2020) 6385–6397, https://doi.org/10.1039/D0CE00928H.

[8] Inas Bouzateur, et al., Lattice constant prediction of complex cubic perovskite A_2BCO_6 using extreme learning machine, in: 2022 International conference of advanced Technology in Electronic and Electrical Engineering (ICATEEE), IEEE, 2022, https://doi.org/10.1109/ICATEEE57445.2022.10093696.

[9] E.T. Chenebuah, M. Nganbe, A.B. Tchagang, Comparative analysis of machine learning approaches on the prediction of the electronic properties of perovskites: a case study of ABX_3 and $A_2BB'X_6$, Mater. Today Commun. 27 (2021) 102462, https://doi.org/10.1016/j.mtcomm.2021.102462.

[10] L. Zhang, L. Mei, K. Wang, et al., Advances in the application of perovskite materials, Nano-Micro Lett. 15 (2023) 177, https://doi.org/10.1007/s40820-023-01140-3.

[11] Nitin Kumar Bansal, et al., Machine learning in perovskite solar cells: recent developments and future perspectives, Energ. Technol. 11 (12) (2023) 2300735, https://doi.org/10.1002/ente.202300735.

[12] Ghulam Dastgeer, et al., A review on recent progress and challenges in high-efficiency perovskite solar cells, Nano Energy 132 (2024) 110401, https://doi.org/10.1016/j.nanoen.2024.110401.

[13] Yong Wang, et al., Lattice mismatch at the heterojunction of perovskite solar cells, Angew. Chem. 136 (29) (2024) e202405878, https://doi.org/10.1002/ange.202405878.

[14] Hamza Bennacer, et al., First principles investigation of optoelectronic properties of $ZnXP_2$ (X= Si, Ge) lattice matched with silicon for tandem solar cells applications using the mBJ exchange potential, Optik 159 (2018) 229–244, https://doi.org/10.1016/j.ijleo.2018.01.079.

[15] I.O. Alade, I.A. Olumegbon, A. Bagudu, Lattice constant prediction of A_2XY_6 cubic crystals (a= K, Cs, Rb, Tl; X= tetravalent cation; Y= F, cl, Br, I) using computational intelligence approach, J. Appl. Phys. 127 (2020) 015303, https://doi.org/10.1063/1.5130664.

[16] M.F. Al-Kuhaili, I.O. Alade, S.M.A. Durrani, Optical constants of hydrogenated zinc oxide thin films, Opt Mater Express 4 (2014) 2323–2331, https://doi.org/10.1364/OME.4.002323.

[17] A. Majid, A. Khan, T.S. Choi, Predicting lattice constant of complex cubic perovskites using computational intelligence, Comput. Mater. Sci. 50 (2011) 1879–1888, https://doi.org/10.1016/j.commatsci.2011.01.035.

[18] R.I. Eglitis, D. Bocharov, S. Piskunov, Ran Jia, Review of first principles simulations of STO/BTO, STO/PTO and SZO/PZO (001) heterostructures, Crystals 13 (2023) 799, https://doi.org/10.3390/cryst13050799.

[19] Y. Zhang, X. Xu, Machine learning lattice constants for cubic perovskite ABX_3 compounds, Chemistry Select 5 (2020) 9999–10009, https://doi.org/10.1002/slct.202002532.

[20] M. Li, C. Dong, H. Zhou, Z. Wang, X. Wang, X. Liang, Y. Lin, N.X. Sun, Characterization of magnetomechanical properties in FeGaB thin films, Appl.Phys.Lett 113 (2018) 262401, https://doi.org/10.1063/1.5065486.

[21] S.T. Ha, C. Shen, J. Zhang, Q. Xiong, Laser cooling of organic–inorganic lead halide perovskites, Nat. Photonics 10 (2016) 115–121, https://doi.org/10.1038/nphoton.2015.243.

[22] K.X. Steirer, P. Schulz, G. Teeter, V. Stevanovic, M. Yang, K. Zhu, J.J. Berry, Defect tolerance in methylammonium lead triiodide perovskite, ACS Energy Lett. 1 (2015) 360–366, https://doi.org/10.1021/acsenergylett.6b00196.

[23] G. Xing, N. Mathews, S.S. Lim, N. Yantara, X. Liu, D. Sabba, M. Grätzel, S. Mhaisalkar, T.C. Sum, Low-temperature solution-processed wavelength-tunable perovskites for lasing, Nat. Mater. 13 (2014) 476–480, https://doi.org/10.1038/nmat3911.

[24] Z.K. Tan, R.S. Moghaddam, M.L. Lai, P. Docampo, R. Higler, F. Deschler, M. Price, A. Sadhanala, L.M. Pazos, D. Credgington, F. Hanusch, Bright light-emitting diodes based on organometal halide perovskite, Nat. Nanotechnol. 9 (2014) 687–692, https://doi.org/10.1038/nnano.2014.149.

[25] W.J. Yin, T. Shi, Y. Yan, Unusual defect physics in CH3NH3PbI3 perovskite solar cell absorber, Appl.Phys.Lett 104 (2014) 063903, https://doi.org/10.1063/1.4864778.

[26] Y. Wang, D. Hasanyan, M. Li, J. Gao, J. Li, D. Viehland, Equivalent magnetic noise in multi- push-pull configuration magnetoelectric composites: model and experiment, IEEE Trans. Ultrason. Ferroelectr. Freq. Control 60 (6) (2013) 1227–1233, https://doi.org/10.1109/TUFFC.2013.2686.

[27] Pierre Hohenberg, Walter Kohn, Inhomogeneous electron gas, Phys. Rev. 136 (3B) (1964) B864, https://doi.org/10.1103/PhysRev.136.B864.

[28] Walter Kohn, Lu Jeu Sham, Self-consistent equations including exchange and correlation effects, Phys. Rev. 140 (4A) (1965) A1133, https://doi.org/10.1103/PhysRev.140.A1133.

[29] E.J. Baerends, P. Sautet, R. van Santen, Basic aspects of density functional theory, in: Computational Methods in Catalysis and Materials Science: An Introduction for Scientists and Engineers, 2009, pp. 23–32, https://doi.org/10.1002/9783527625482.ch2.

[30] Sabagh Moeini, Fatemeh Shariatmadar Alireza, Tehrani, and Alireza Naeimi-Sadigh., Machine learning-driven band gap prediction/classification and feature importance analysis of inorganic perovskites, Int. J. Energy Res. 2025 (1) (2025) 9974355, https://doi.org/10.1155/er/9974355.

[31] Abdullah Alharthi, et al., Improving the interpretability of ANN-based predictions of lattice constants in Aliovalently doped perovskites using partial dependence plots, Crystals 15 (6) (2025) 538, https://doi.org/10.3390/cryst15060538.

[32] Bryan Wright, Rick Ubic, Empirical models for predicting cubic/pseudocubic lattice parameters of perovskites, Mater. Res. Bull. 185 (2025) 113318, https://doi.org/10.1016/j.materresbull.2025.113318.

[33] Soundous Touati, et al., Predictive machine learning approaches for perovskites properties using their chemical formula: towards the discovery of stable solar cells materials, Neural Comput. & Applic. 36 (26) (2024) 16319–16329, https://doi.org/10.1007/s00521-024-09992-5.

[34] Taizhong Yao, et al., Discovering ABO3-type perovskite with different dielectric constants via intelligent optimization algorithm, AIP Adv. 14 (7) (2024), https://doi.org/10.1063/5.0210811.

[35] Sabagh Moeini, Fatemeh Shariatmadar Alireza, Tehrani, and Alireza Naeimi-Sadigh., Machine learning-enhanced band gaps prediction for low-symmetry double and layered perovskites, Sci. Rep. 14 (1) (2024) 26736, https://doi.org/10.1038/s41598-024-77081-7.

[36] D.O. Obada, et al., Explainable machine learning for predicting the band gaps of ABX_3 perovskites, Mater. Sci. Semicond. Process. 161 (2023) 107427, https://doi.org/10.1016/j.mssp.2023.107427.

[37] Sams Jarin, et al., Predicting the crystal structure and lattice parameters of the perovskite materials via different machine learning models based on basic atom properties, Crystals 12 (11) (2022) 1570, https://doi.org/10.3390/cryst12111570.

[38] Qiuling Tao, et al., Machine learning for perovskite materials design and discovery, npj Comput. Mater. 7 (1) (2021) 23, https://doi.org/10.1038/s41524-021-00495-8.

[39] Jeric Briones, Mark Christian Guinto, Christian Mark Pelicano, Accelerated lattice constant prediction of perovskite materials (ABX_3, $A_2BB'O_6$) using partial least squares and principal component regression methods, Mater. Lett. 298 (2021)

130040, https://doi.org/10.1016/j.matlet.2021.130040.
[40] Yuxin Li, et al., Mlatticeabc: generic lattice constant prediction of crystal materials using machine learning, ACS Omega 6 (17) (2021) 11585–11594.
[41] Yun Zhang, Xu. Xiaojie, Machine learning lattice constants from ionic radii and electronegativities for cubic perovskite a 2 XY 6 compounds, Phys. Chem. Miner. 47 (9) (2020) 39, https://doi.org/10.1007/s00269-020-01108-4.
[42] Logan Williams, Arpan Mukherjee, Krishna Rajan, Deep learning based prediction of perovskite lattice parameters from hirshfeld surface fingerprints, J. Phys. Chem. Lett. 11 (17) (2020) 7462–7468, https://doi.org/10.1021/acs.jpclett.0c02201.
[43] Juan Wang, et al., Studying the thermodynamic phase stability of organic–inorganic hybrid perovskites using machine learning, Molecules 29 (13) (2024) 2974, https://doi.org/10.3390/molecules29132974.
[44] Lucas Foppa, et al., Hierarchical symbolic regression for identifying key physical parameters correlated with bulk properties of perovskites, Phys. Rev. Lett. 129 (5) (2022) 055301, https://doi.org/10.1103/PhysRevLett.129.055301.
[45] Soo Min Kim, et al., Optical characterization and prediction with neural network modeling of various stoichiometries of perovskite materials using a hyperregression method, Nanomaterials 12 (6) (2022) 932, https://doi.org/10.3390/nano12060932.
[46] Ruoting Zhao, et al., Evaluation of performance of machine learning methods in mining structure–property data of halide perovskite materials, Chin. Phys. B 31 (5) (2022) 056302, https://doi.org/10.11922/sciencedb.01611.
[47] Jiechun Liang, et al., Accelerating perovskite materials discovery and correlated energy applications through artificial intelligence, Energy Mater 2 (3) (2022) 200016, https://doi.org/10.20517/energymater.2022.14.
[48] Yun Zhang, Xu. Xiaojie, Modeling of lattice parameters of cubic perovskite oxides and halides, Heliyon 7 (7) (2021), https://doi.org/10.1016/j.heliyon.2021.e07601.
[49] Wissam A. Saidi, Waseem Shadid, Ivano E. Castelli, Machine-learning structural and electronic properties of metal halide perovskites using a hierarchical convolutional neural network, npj Comput. Mater. 6 (1) (2020) 36, https://doi.org/10.1038/s41524-020-0307-8.
[50] Yun Zhang, Xu. Xiaojie, Machine learning lattice constants for cubic perovskite A2XY6 compounds, J. Solid State Chem. 291 (2020) 121558, https://doi.org/10.1016/j.jssc.2020.121558.
[51] Ibrahim Olanrewaju Alade, Yun Zhang, Xu. Xiaojie, Modeling and prediction of lattice parameters of binary spinel compounds (AM_2X_4) using support vector regression with Bayesian optimization, New J. Chem. 45 (34) (2021) 15255–15266, https://doi.org/10.1039/D1NJ01523K.
[52] O. Castillo, et al., A survey on type-3 fuzzy logic systems and their control applications, IEEE/CAA J. Autom. Sin. 11 (8) (2024) 1744–1756, https://doi.org/10.1109/JAS.2024.124530.
[53] Anupam Kumar, Ritu Raj, Ardashir Mohammadzadeh, Recent advancements in type-3 fuzzy logic systems: a comprehensive review, IEEE Trans. Emerg. Topics Comput. Intell. (2024), https://doi.org/10.1109/TETCI.2024.3433514.
[54] Shu-Rong Yan, Ardashir Mohammadzadeh, Ebrahim Ghaderpour, Type-3 fuzzy logic and Lyapunov approach for dynamic modeling and analysis of financial markets, Heliyon 10 (13) (2024), https://doi.org/10.1016/j.heliyon.2024.e33730.
[55] Oscar Castillo, Patricia Melin, Type-3 fuzzy prediction, in: Type-3 Fuzzy Logic in Time Series Prediction, Springer Nature Switzerland, Cham, 2024, pp. 1–4, https://doi.org/10.1007/978-3-031-59714-5.
[56] Oscar Castillo, Juan R. Castro, Patricia Melin, Interval type-3 fuzzy aggregation of neural networks for multiple time series prediction: the case of financial forecasting, Axioms 11 (6) (2022) 251, https://doi.org/10.3390/axioms11060251.
[57] Oscar Castillo, et al., Interval type-3 fuzzy aggregators for ensembles of neural networks in COVID-19 time series prediction, Eng. Appl. Artif. Intell. 114 (2022) 105110, https://doi.org/10.1016/j.engappai.2022.105110.
[58] Patricia Melin, et al., Design of type-3 fuzzy systems and ensemble neural networks for COVID-19 time series prediction using a firefly algorithm, Axioms 11 (8) (2022) 410, https://doi.org/10.3390/axioms11080410.
[59] Oscar Castillo, Juan R. Castro, Patricia Melin, Forecasting the COVID-19 with interval type-3 fuzzy logic and the fractal dimension, Int. J. Fuzzy Syst. 25 (1) (2023) 182–197, https://doi.org/10.1007/s40815-022-01351-7.
[60] Oscar Castillo, Martha Pulido, Patricia Melin, Interval type-3 fuzzy aggregators for ensembles of neural networks in time series prediction, in: International Conference on Intelligent and Fuzzy Systems, Springer International Publishing, Cham, 2022, https://doi.org/10.1007/978-3-031-09173-5_90.
[61] Anirban Tarafdar, et al., Prediction of eco sustainability component using fuzzy Z numbers based ratio analysis and interval type 3 fuzzy logic system, J. Clean. Prod. 481 (2024) 144125, https://doi.org/10.1016/j.jclepro.2024.144125.
[62] Anirban Tarafdar, et al., Enhancing intrusion detection using wireless sensor networks: a novel ahp-madm aggregated multiple type 3 fuzzy logic-based k-barriers prediction system, Peer Peer Netw. Appl. 17 (3) (2024) 1732–1749, https://doi.org/10.1007/s12083-024-01688-w.
[63] Inas Bouzateur, et al., A new ANN-PSO framework to chalcopyrite's energy band gaps prediction, Mater. Today Commun. 34 (2023) 105311, https://doi.org/10.1016/j.mtcomm.2023.105311.
[64] Nadav Cohen, Itzik Klein, Adaptive Kalman-informed transformer, Eng. Appl. Artif. Intell. 146 (2025) 110221, https://doi.org/10.1016/j.engappai.2025.110221.
[65] Vogt, Moritz D. Pinheiro-Torres, et al., 2024 IEEE Congress on Evolutionary Computation (CEC). FlexKalmanNet: a modular AI-enhanced Kalman filter framework applied to spacecraft motion estimation, IEEE, 2024, https://doi.org/10.1109/CEC60901.2024.10612159.
[66] Assefinew Wondosen, et al., Bayesian optimization for fine-tuning EKF parameters in UAV attitude and heading reference system estimation, Aerospace 10 (12) (2023) 1023, https://doi.org/10.3390/aerospace10121023.
[67] Chanthol Eang, Seungjae Lee, An integration of deep neural network-based extended Kalman filter (DNN-EKF) method in ultra-wideband (UWB) localization for distance loss optimization, Sensors 24 (23) (2024) 7643, https://doi.org/10.3390/s24237643.
[68] Hend M. Fahmy, et al., Hybrid extended Kalman filter with Newton Raphson method for lifetime prediction of lithium-ion batteries, Sci. Rep. 15 (1) (2025) 14592, https://doi.org/10.1038/s41598-025-91156-z.
[69] Hamed Danandeh Hesar, Amin Danandeh Hesar, Adaptive dual augmented extended Kalman filtering of ECG signals, Measurement 239 (2025) 115457, https://doi.org/10.1016/j.measurement.2024.115457.
[70] Tasadeek Hassan Dar, Satyavir Singh, Advanced integration of bidirectional long short-term memory neural networks and innovative extended Kalman filter for state of charge estimation of lithium-ion battery, J. Power Sources 628 (2025) 235893, https://doi.org/10.1016/j.jpowsour.2024.235893.
[71] Guangshun Fu, et al., Axial temperature distribution estimation of induction motor slot conductors using a fractional-order thermal diffusion model and extended Kalman filter, Appl. Therm. Eng. (2025) 126831, https://doi.org/10.1016/j.applthermaleng.2025.126831.
[72] Xiaoyu Han, et al., CBGTE: neural network aided extended Kalman filter for dual-band infrared attitude estimation, IEEE Trans. Autom. Sci. Eng. (2025), https://doi.org/10.1109/TASE.2025.3561781.
[73] Sultan Noman Qasem, et al., A type-3 logic fuzzy system: optimized by a correntropy based Kalman filter with adaptive fuzzy kernel size, Inf. Sci. 572 (2021) 424–443, https://doi.org/10.1016/j.ins.2021.05.031.
[74] Javad Faraji, Jafar Keighobadi, Farrokh Janabi-Sharifi, Design and implementation of an adaptive extended Kalman filter with interval type-3 fuzzy set for an attitude and heading reference system, Signal Process. 233 (2025) 109947, https://doi.org/10.1016/j.sigpro.2025.109947.
[75] Javad Faraji, Jafar Keighobadi, Farrokh Janabi-Sharifi, Design and implementation of an adaptive unscented Kalman filter with interval Type-3 fuzzy set for an attitude and heading reference system considering gyroscope bias, Mech. Syst. Signal Process. 223 (2025) 111870, https://doi.org/10.1016/j.ymssp.2024.111870.
[76] Qingde Sun, Wan-Jian Yin, Thermodynamic stability trend of cubic perovskites, J. Am. Chem. Soc. 139 (42) (2017) 14905–14908, https://doi.org/10.1021/jacs.7b09379.
[77] Christopher J. Bartel, et al., New tolerance factor to predict the stability of perovskite oxides and halides, Sci. Adv. 5 (2) (2019) eaav0693, https://doi.org/10.1126/sciadv.aav0693.
[78] Taoreed O. Owolabi, Extreme learning machine and swarm-based support vector regression methods for predicting crystal lattice parameters of pseudo-cubic/cubic perovskites, J. Appl. Phys. 127 (24) (2020), https://doi.org/10.1063/5.0008809.
[79] V. Sidey, A simplified empirical model for predicting the lattice parameters of the cubic/pseudocubic perovskites, J. Solid State Chem. 279 (2019) 120951, https://doi.org/10.1016/j.jssc.2019.120951.
[80] Samir Zeghlache, et al., "Backstepping sliding mode control based on adaptive type-3 fuzzy system of a transformable quadcopter." international journal of, Dyn. Control. 13 (7) (2025) 1–33, https://doi.org/10.1007/s40435-025-01774-8.
[81] Erdal Kayacan, Mojtaba Ahmadieh Khanesar, Chapter 6 - extended Kalman filter algorithm for the tuning of type-2 fuzzy neural networks, in: Fuzzy Neural Networks for Real Time Control Applications, 2016, pp. 71–84, https://doi.org/10.1016/B978-0-12-802687-8.00006-2.
[82] Cong Hung Do, Huei-Yung Lin, Incorporating neuro-fuzzy with extended Kalman filter for simultaneous localization and mapping, Int. J. Adv. Robot. Syst. 16 (5) (2019) 1729881419874645, https://doi.org/10.1177/1729881419874645.
[83] Artun Sel, et al., Comparative study of an EKF-based parameter estimation and a nonlinear optimization-based estimation on PMSM system identification, Energies 14 (19) (2021) 6108, https://doi.org/10.3390/en14196108.
[84] Simuck F. Yuk, et al., Putting error bars on density functional theory, Sci. Rep. 14 (1) (2024) 20219, https://doi.org/10.1038/s41598-024-69194-w.
[85] Qianyu You, Gu Shun, Xiaofan Gou, The highly accurate interatomic potential of CsPbBr3 perovskite with temperature dependence on the structure and thermal properties, Materials 16 (5) (2023) 2043, https://doi.org/10.3390/ma16052043.